Published in : International Journal of Biological Macromolecules (2024), n°279 (Pt 4), 135571
DOI: 10.1016/j.ijbiomac.2024.135571
Status : Postprint (Author's version)

CELLULOSE NANO-DISPERSIONS ENHANCED BY ULTRASOUND ASSISTED CHEMICAL MODIFICATION DRIVE OSTEOBLAST PROLIFERATION AND DIFFERENTIATION IN PVA/HA BONE TISSUE ENGINEERING SCAFFOLDS

Shunshun Zhu[a], Hongnan Sun[a,*], Taihua Mu [a,*], Aurore Richel[b]

[a] *Laboratory of Food Chemistry and Nutrition Science, Institute of Food Science and Technology, Chinese Academy of Agricultural Sciences, Key Laboratory of Agro- Products Processing, Ministry of Agriculture and Rural Affairs, No. 2 Yuan Ming Yuan West Road, Haidian District, P.O. Box 5109, Beijing 100193, China*
[b] *University of Liège, Gembloux Agro-Bio Tech, Laboratory of Biomass and Green Technologies, Passage des Déportés, 2, 5030 Gembloux, Belgium*

ARTICLE INFO

Chemical compounds studied in this article:

Glacial acetic acid (PubChem CID: 176) Hydrochloric acid (PubChem CID: 313) Phosphoric acid (PubChem CID: 1004) Calcium hydroxide (PubChem CID: 6093208) Sodium hydroxide (PubChem CID: 14978) Sodium chlorite (PubChem CID: 23668197)

KEYWORDS: Cellulose nanocrystals**;** Hydroxyapatite**;** Bone tissue engineering scaffold

ABSTRACT

To develop a biological bone tissue scaffold with uniform pore size and good cell adhesion was both challenging and imperative. We prepared modified cellulose nanocrystals (CNCs) dispersants (K-PCNCs) by ultrasound- assisted alkylation modification. Subsequently, nano-hydroxyapatite (HC-K) was synthesized using K-PCNCs as a dispersant and composited with polyvinyl alcohol (PVA) to prepare the scaffold using the ice template method. The results showed that the water contact angle and degree of substitution (135°, 1.53) of the K-PCNCs were highest when the ultrasound power was 450 W and the time was 2 h. The dispersion of K-PCNCs prepared under this condition was optimal. SEM showed that the pore distribution of the composite scaffolds was more homogeneous than the PVA scaffold. The porosity, equilibrium swelling rate, and mechanical properties of the composite scaffolds increased and then decreased with the increase of HC-K content, and reached the maximum values (56.1 %, 807.7 %, and 0.085 ± 0.004 MPa) at 9 % (*w*/w) of HC-K content. Cell experiments confirmed scaffold has good cytocompatibility and mineralization capacity. The ALP activity reached 1.71 ± 0.25 (ALP activity/mg protein). In conclusion, the scaffolds we developed have good biocompatibility and mechanical properties and have great potential in promoting bone defect repair.

* Corresponding authors.

E-mail addresses: sunhongnan@caas.cn (H. Sun), mutaihua@126.com (T. Mu).

Introduction

Although the bones in the human body can heal themselves, large bone defects need bone transplantation, which leads to an elevated risk of immune rejection [1]. Bone tissue engineering scaffolds have been proven to achieve the purpose of bone defect repair with minimal risk (low infectivity and low carcinogenicity, reduced immune rejection). Porous bone scaffolds based on biopolymers (such as polyvinyl alcohol, PVA) and bioceramics (such as hydroxyapatite, HA) have been proven to promote the growth of bone cells and the formation of new bone tissues [2,3]. PVA composite material is easy to change its shape has high flexibility and can adjust the surface and internal factors of the scaffold, so it can be used as a new scaffold material to promote tissue development and regeneration [4]. PVA also can produce high-density porous structures and provide scaffolds for the growth and differentiation of osteoblasts [5,6]. The main challenge in designing PVA-based scaffolds is to maintain good mechanical properties, high porosity, and anti-infection ability [7]. Poor mechanical performance and infection at the site of scaffold implantation are issues that lead to scaffold failure.

Natural (organic or inorganic) structures such as polysaccharides and HA offer superiority in the targeted design of prepared scaffold structures. Moreover, osteoblasts can recognize and interact with specific biomaterials (such as HA), because the amino acids and mono- saccharides in these materials have the same binding regions as the receptors on the surface of osteoblasts [8]. HA is a vital component of natural bone, accounting for up to 50 %. Consequently, owing to its capacity to enhance the proliferation and differentiation of osteoblastic cells, HA has emerged as a significant biomaterial for the fabrication of bone scaffolds [9]. Based on this, some studies have combined PVA with HA to prepare composite scaffolds. Ashraf et al. (2019) found that HA nanoparticles as an adjuvant can enhance the bioactivity of PVA scaffolds [10]. Due to its biocompatibility and bone conductivity, HA can accelerate the reconstruction of damaged hard tissue [11,12]. Methods for uniform distribution of HA in polymer matrices include in situ mineralization techniques, wet chemical precipitation, or pyrolysis.

Abbreviations

AFM	Atomic force microscopy
ALP	Alkaline phosphatase
CCNCs	Commercial cellulose nanocrystals
CNCs	Cellulose nanocrystals
DS	Degree of substitution
DSC	Differential scanning calorimetry analysis
DTG	Derived thermogravimetric
FTIR	Fourier transform infrared spectroscopy
HA	Hydroxyapatite
HC-C	Hydroxyapatite synthesized with commercial cellulose nanocrystals as a dispersant
HC-K	Hydroxyapatite synthesized with
PHC-C	Hydroxyapatite synthesized with commercial cellulose nanocrystals as dispersant/polyvinyl alcohol bone tissue engineering scaffold
C-HA	Commercial hydroxyapatite/polyvinyl alcohol bone tissue engineering scaffold
PHC-K	Hydroxyapatite synthesized with alkylated modified cellulose nanocrystals as dispersant/polyvinyl alcohol bone tissue engineering scaffold
PHC-P	Hydroxyapatite synthesized with purple sweet potato peel residues cellulose nanocrystals as dispersant/polyvinyl alcohol bone tissue engineering scaffold
PVA	Polyvinyl alcohol
SEM	Scanning electron microscopy
TEM	Transmission electron microscopy

	alkylated modified cellulose nanocrystals as the dispersant	TG	Thermogravimetric
HC-P	Hydroxyapatite synthesized with purple sweet potato peel residues cellulose nanocrystals as the dispersant	TGA	Thermogravimetric analysis
		WCA	Water contact angle
K-PCNCs	Alkylated modified purple sweet potato peel residue cellulose nanocrystals	XRD	X-ray diffractometer
		XPS	X-ray photoelectron spectroscopy
PCNCs	Purple sweet potato peel residue cellulose nanocrystals		

[13-16] However, these methods produced HA with poor crystallinity or in aggregated and agglomerated forms, affecting the dispersibility and mechanical properties of the scaffold materials [17-19]. To address these constraints, dispersants were employed to enhance the colloidal stability and crystallinity of HA [14].

Cellulose, an organic biomass material, is abundant in nature and serves as the most prevalent renewable polymer and polysaccharide [20,21]. Cellulose nanocrystals (CNCs) are nanoscale biomaterials derived from cellulose [11,16]. It possesses characteristics such as high crystallinity, thermal stability, and biodegradability, alongside significant physicochemical properties attributed to the nanometer scale. It has been documented that the dispersibility and colloidal stability of HA particles were significantly enhanced through the utilization of CNCs as an environmentally friendly dispersant. [22]. In addition to providing mechanical properties, the wide colloidal distribution of CNCs in the PVA matrix has been fully proven to have biocompatibility, high mechanical resistance, and crystallization rate [23]. At the same time, the application of HA/CNCs in transparent coating materials was studied, and it was found that the distribution and crystallinity of HA were further improved [24]. Niamsap et al. (2019) synthesized bacterial nanocellulose/HA/CNCs composites in situ using CNCs, which showed dispersion of HA on CNCs particles with a Ca/P ratio of 1.66 and improved distribution and crystallinity of HA [25]. Therefore, CNCs can be utilized as a bio-dispersant for HA synthesis, facilitating bone defect repair. However, CNCs pose a challenge in dispersing into hydrophobic matrices due to its hydrophilicity and polyhydroxy functional groups, limiting its application as a dispersant.

Surface functionalization has been proven to be an economical way to improve the performance and function of CNCs. Hydroxyl groups provide a good platform for surface functionalization [26]. Chemical modifications such as grafting, acetylation, esterification, etherification, or alkylation are used to tailor the surface chemistry of CNCs to enhance interfacial compatibility with polymer matrices and at the same time improve the stability of the composites [27]. The alkylation modification technology contains active primary amine groups and hydrophobic alkane long chains, which can catalyze the mutual reaction between amine groups and hydroxyl groups, effectively improving the hydrophobicity of CNCs suspensions [28]. Simple and convenient engineering techniques are more conducive to applying alkylation modification technology in large-scale industries [29]. Esmizadeh et al. (2024) showed that by modifying CNCs with dodecyl succinic anhydride, the modified CNCs also exhibited excellent dispersion in hydrophobic

polymers, such as polyurethane and ethylene propylene diene rubber [30]. Similarly, Wu et al. (2020) prepared cellulose III nanocrystals using 3-aminopropyltriethoxysilane (KH-550) as an alkylated substrate, with further improvement in dispersion and reduction in crystallinity [31]. Therefore, it is important to use alkylation-modified CNCs to improve the dispersibility of CNCs. However, chemical modification methods designed to functionalize CNCs in hydrophobic environments have so far been insufficient and unsatisfactory, as most of them result in the lowest degree of substitution (DS) [32]. The range of DS values reported in the literature is 0.1-1 [33,34]. DS is critical to the degree of chemical reaction.

Ultrasonic waves serve as an efficient and rapid physicochemical method involving cavitation reactions and chemical actions, which can break down the connection network of macromolecules into smaller molecules [20]. The ultrasonic waves processing uses frequencies between 20 and 100kHz, with powers ranging from 240

to 1200W in the liquid phase, where microbubbles form and subsequently collapse caused by the high level of turbulence and shear stress, thereby promoting depolymerization of polymers [35]. It has been shown that depolymerization of cellulose occurs due to the process of cavitation and collapse of bubbles. When ultrasonic waves energy was applied to carbohydrates, the straight or branched chains of the compounds would undergo pressure changes and shear, breaking the polymer chains into monomeric units [36]. The free radicals generated during ultrasonic treatment result in the breaking of glycosidic bonds present in cellulose, and this provides a relevant site for the reactive binding of alkylating groups to the hydroxyl groups of CNCs [37].

To the best of our knowledge, previous studies have focused on the modification of CNCs using only physical (e.g., mechanical grinding, ultrasonic treatment, etc) or chemical methods (e.g., alkylation, etherification, etc.), with low DS obtained from this modification methods, and the use of a combination of ultrasound-enhanced alkylation to change DS has not been reported. In addition, the modified CNC prepared by ultrasound-enhanced modified composite method was used to synthesize HA, and the composite of HA and biopolymers was used to prepare bone tissue engineering scaffolds, whose cytocompatibility and mineralized osteogenic ability and their wide application in the field of bone defect repair have not been fully explored.

In this study, the effects of ultrasonic treatment time and power on the water contact angle (WCA) and DS of ultrasonic-assisted alkylation- modified CNCs were investigated, and the physicochemical properties and multiscale structure of the alkylation-modified CNCs were

evaluated, based on which the effects of the HA concentration synthesized from the alkylated CNCs on the mechanical properties, crystalline, biocompatibility and mineralization ability of the PVA/HA scaffolds were investigated. The purpose of this study was to determine whether PVA/HA bilayer scaffolds could be used as potential scaffolds for the in vitro treatment of osteogenesis imperfecta. The findings provide a theoretical basis for ultrasound-assisted chemical modification of CNCs and a scientific basis for the application of bio-based bone tissue engineering scaffolds in bone defect repair.

Materials and methods

MATERIALS AND REAGENTS

Phosphoric acid (purity: ≥85 wt%), calcium hydroxide (purity: ≥95 %), polyvinyl alcohol (PVA, purity: 99 %), commercial HA (purity: 99 %), and 3-aminopropyltriethoxysilane (silane coupling agent-KH-550, purity: 98 %) were purchased from Sigma-Aldrich, Inc. (St. Louis, MO, USA). Cell reagents were purchased from Thermo Fisher Scientific, Inc. (Beijing, China). Commercial CNCs (purity: 99 %, CCNCs) were purchased from Science K Company (Hu'zhou, Zhejiang, China). Other chemicals were of analytical grade. Deionized water was used in these experiments.

PCNCS PREPARATION

CNCs were prepared according to previous laboratory methods: maleic acid hydrolysis of purple sweet potato peel residue cellulose was carried out in a 75 % (w/w) concentration maleic acid solution. The mass ratio of maleic acid to purple potato peel residue cellulose was 10: 1 (w/w), and continuous ultrasonic treatment (KQ-500DE Ultrasonic Cleaner, Kunshan Ultrasonic Instrument Co., Ltd.) for 1 h (at an ultrasonic treatment power of 475 W, 50 Hz). Then, the acid hydrolysis process was continued at 110 ◦C for 2 h, then freeze-dried to obtained (denoted by PCNCs) [38].

ALKYLATED PCNCS PREPARATION

The alkylated PCNCs (K-PCNCs) were prepared following the methodology described by Wu et al. (2020) with slight modifications [31]. PCNCs (0.4 g) were ultrasonically dispersed in 50.0 mL of ethanol solution. Then, a 10 % (w/w) silane coupling agent-KH-550 working solution was prepared. Glacial acetic acid was used to adjust the pH (4-5), and an ultrasonic-assisted reaction was carried out at room temperature. Then, absolute ethanol (20 mL) was added to terminate the reaction, and the product was dialyzed in a dialysis bag (MW: 7000-14,000 Da) and deionized water for one week until the pH value was stable and reached 7. Finally, the dialyzed suspension was lyophilized and alkylated to modify CNCs.

NANOCOMPOSITE PREPARATION

The nanocomposites were prepared following the methodology described by Lam et al. (2022) [39] with some modifications. A 0.3 % suspension of CNCs (CCNCs, PCNCs, and K-PCNCs) was poured into 1 M calcium hydroxide (100 mL, pH 10) and stirred evenly for 1 h at 60 °C. Then, 0.6 M phosphoric acid was added dropwise in uniform dispersion for 5 h. After the addition of phosphoric acid, the reaction was continued for 24 h (27 °C), then washed with distilled water until the pH reached 7.

SCAFFOLD PREPARATION

The scaffolds were prepared following the methodology described by Lam et al. [39] with slight modifications. 3, 6, 9, and 12 % (w/v, 50 mL) of the HA were mixed with 5 % (w/v, 50 mL) PVA for 3 h, after which the reaction was stirred. Subsequently, the bubbles in the mixed solution

were removed by ultrasonic treatment for 20 min, and the suspension was poured onto a 6-well plate and freeze-dried at -60 °C.

DISPERSIBILITY ANALYSIS

Freeze-dried PCNCs and K-PCNCs were redispersed in distilled water, absolute ethanol, and toluene at a concentration of 0.2 % (w/w) by ultrasonic treatment for 1 h [31]. Sonication was carried out at 5 % amplitude. Before observation, the samples stood for 2 weeks.

POROSITY AND EQUILIBRIUM SWELLING RATE ANALYSIS

The porosity of the scaffolds was estimated with ethanol as the solvent following the method of Lan et al. [40] with slight modifications. The samples were immersed for 72 h.

$$\text{Porosity (\%)} - \frac{V_1 \quad V_3}{V_2 \quad V_3} \times 100 \qquad (1)$$

where V_1 is the volume of ethanol, V_2 is the volume of ethanol and sample, and V3 is the volume of ethanol remaining after removing the sample.

The equilibrium swelling rate of the scaffolds was estimated for 24 h, and the difference between the constant weight (Wdry) and the dissolved weight in phosphate buffer solution (PBS, 0.01 M) was divided by the constant weight (Wdry) of the scaffold.

$$\text{Equilibrium swelling rate (\%)} = \frac{W_{swollen} - W_{dry}}{W_{dry}} \times 100 \qquad (2)$$

CHARACTERIZATION

The substitution degree was determined by a solid-state ^{13}C nuclear magnetic resonance analysis (NMR) spectrometry probe (Bruker Advance III HD 400 MHz spectrometer, Germany). The spectrometer has channels of ^{13}C at 100.5 and 400 MHz. We calculated DS from the NMR spectra using the method described by Wu et al. [41] with slight modifications.

Contact angle analyzers (Bruker Alicona OCA200, Sweden) were used to analyze the WCA of the samples. The sample solution was coated on the surface of the silicon wafer by the impregnation method. The test water volume was 1 µL.

The hydrocolloidal stability of the samples was determined by a Malvin nanoparticle size analyzer (Malvin Mastersizer 2000, England). Briefly, the samples were diluted to 2 mg/mL and dispersed in deionized water (25 °C) and scattering angle of 173°.

The morphology of the scaffolds was examined by scanning electron microscopy (SEM) (Hitachi Regulus 8100, Japan). The scaffolds were adhered to a conductive carbon tape and a sputter coater was used to deposit gold particles on the surface of the scaffolds under vacuum. EDS combined with SEM to determine the sample's elemental composition. The pore size of the scaffolds was calculated using Image J software (Java 1.8.0_172, USA). The modified CNCs and HA suspension were imaged by transmission electron microscopy (TEM) (HITACHI H-7650, Japan). A drop of the sample suspension was cast on a copper grid with carbon coating, washed with a few drops of Milli-Q water, dried at room temperature and imaged by TEM.

Atomic force microscopy (AFM) observation (Multimode 8, Bruker Company, Germany) of the samples was prepared by placing a few drops of CNCs with 0.005 % (w/w) solution onto a square of freshly cleaved mica and then air-dried overnight.

Differential scanning calorimetry analysis (DSC) analysis of the samples was carried out on a calorimeter (DSC Q100, TA Instruments, New Castle, DE, USA) over 25 to 250 °C at a heating rate of 5 °C per minute.

The thermal stability of the samples was tested by thermogravimetric (TG) analysis (Discovery TGA550 USA). 10 mg samples were weighed

into the TG analyzer at room temperature. The measurement conditions were 40 mL/min, with a temperature increase rate of 10 K/min.

X-ray photoelectron spectroscopy (XPS) analysis (AXIS SUPRA+ AXIS NOVA AMICUS, Japan) was performed using the AXIS Supra system. The system used a 500 mm Roland Circle monochromatic Al K-a (1486.6 eV) source and a combined hemispherical and spherical mirror analyzer (HSA/SMA). High-resolution scans were collected in steps of 0.1 eV.

Fourier transform infrared spectroscopy (FTIR) analysis was 1 g sample mixed with 50-60 mg of potassium bromide powder in an agate mortar. The spectra were recorded on an FTIR-650 (Tianjin Guangdong Science and Technology Development Co. Ltd.).

X-ray diffractometer (XRD) (Bruker Corp., Billerica, MA, USA) was used to scan the sample with Cu-Ka radiation (X = 0.15418 nm). 20 mg of each sample was scanned at 29 = 3-50° (scanning speed: 2°/min; voltage: 40 kV; the current: 40 mA).

The mechanical properties of the samples were tested by a universal testing machine (Shimadzu model AGS5kN, Japan) and the samples were prepared using the method described by Lan et al. [41] with slight modifications. Briefly, a load cell of 1 kN was applied on a cylindrically shaped (10 x 10 mm) of the scaffolds.

CELL CYTOTOXICITY AND CELL VIABILITY ANALYSIS

The scaffolds were sterilized by UV light and immersed in MC3T3- E1osteoblast a-minimum essential medium supplemented with 1 % primocin [39]. The cytotoxicity of bone tissue engineering scaffolds was evaluated. MC3T3-E1 osteoblasts were seeded on a 96 well-plate at a density of 30,000 cells/cm^2 and placed in a 37 °C/5 % CO2 incubator for 24 h. Added appropriately sized scaffolds to the culture medium and incubate the cells for 24 h. Cells without scaffolds were used as negative controls. In all experiments, MTS reagent (100 mL) was added at a ratio of 10:1 and cultured at 37 ˚C/5 % CO_2 for 2 h. The optical density value was measured on a microplate using an absorbance of 490 nm. The medium without cell inoculation was used as a blank control. After 1, 4, 7, and 10 d, MTS was used to evaluate the cell proliferation on the scaffold. MC3T3-E1 osteoblasts were seeded on the scaffolds. The seeding density was 30,000 cells/cm^2. The culture medium without inoculated cells was a blank control. The corrected absorbance was obtained by subtracting the absorbance value at 490 nm from the respective blank readings. The cell viability on the scaffolds was compared with the data recorded on PVA.

MC3T3-E1 osteoblasts were seeded on the scaffolds at 30,000 cells/ cm^2 and cultured in an osteogenic medium containing p-glycerophosphate (10 mM) and L-ascorbic acid (50 mg/mL) for 14 d. The alkaline phosphatase (ALP) activity was determined by a colorimetric analysis kit (ab83369, Abcam). Briefly, cell culture media were collected after 4, 7, 10, and 14 d. The samples were incubated with *p*-nitrophenyl phosphate for 60 min (25 °C). After the addition of the solution was stopped, the absorbance was measured at 405 nm using a microplate reader to determine the total protein content of the cells and the ALP activity of the scaffolds.

IN VITRO DEGRADATION

The in vitro degradation experiments were carried out according to ISO 10993-13:2010 [42]. The scaffolds (10 x 10 x 0.5 mm^3) were incubated (1 g/30 mL) at 37 ˚C in an oxidizing environment, with an aqueous solution of hydrogen peroxide (10 %) and 1.31 mM of calcium chloride. Before and after the degradation test, the specimens were dried to a constant weight to determine weight loss, expressed as

$$\text{Degradation rate}(\%) = \frac{W_t - W_0}{W_0} \times 100 \qquad (3)$$

where W_t represents the sample weight after an immersion time t and W_0

is the initial weight of the dry sample before immersion.

To further determine the degradation rate of the scaffold in a simulated in vivo environment, the degradation rate of the scaffolds was determined in phosphate buffer solution (PBS) at pH 7.4 at room temperature [43]. The scaffolds were weighed and placed in PBS, then periodically removed from the solution and weighed, and the scaffolds were dried at 37 °C for 24 h. The PBS solution was changed daily. The calculation formula remained as Eq. (3).

STATISTICAL ANALYSIS

Data were presented as the means ± standard deviations from at least three independent samples. All the results were analyzed using SPSS 26.0 software (IBM, Armonk, NY, USA) and GraphPad Prism 9 software (Dotmatics, USA) for one-way ANOVA. In all cases, the criterion for statistical significance was $p < 0.05$.

Results and discussion

EFFECT OF DIFFERENT ULTRASONIC TREATMENT TIMES AND POWER ON WCA AND DS OF K-PCNCS

Fig. 1a showed the modification of PCNCs (R refers to the grafted groups or H according to the DS). As shown in Fig. 1b and c, ultrasonic treatment time significantly affected the WCA and the DS of K-PCNCs. With increased ultrasonic time treatment (<2 h), the WCA and DS of K- PCNCs gradually increased. When the ultrasonic time was 1.5 h, the WCA reached a maximum of 134.05°. When the ultrasonic time was 2 h, the DS reached a maximum of 1.49, and the WCA of K-PCNC increased by 61° and the DS by about 0.3 compared to modified PCNC which ultrasound was not added. When the ultrasonic treatment time was >1.5 h, the WCA decreased, and there was no significant difference between the 1.5 h ultrasonic treatment group and the 2 h ultrasonic group. Compared with the WCA of K-PCNCs without ultrasonic treatment, the WCA and the DS of K-PCNCs with ultrasonic treatment were significantly improved, indicating that ultrasonic waves were an effective way to catalyze the modification process and enhanced the reaction degree of hydroxylation between alkylation reagent and PCNCs. Compared with alkylated chitosan (92.53°) [44], the WCA of ultrasound-assisted K- PCNCs was increased by 18.37°. Aureliano et al. showed a decrease in the polydispersity of cellulose crystals after sonication, indicating a more homogeneous size of the cellulose crystals, as the medium to high- intensity ultrasound power applied in a brief period helped to break down the cellulose structure [45]. The ultrasound treatment process promoted hydrodynamic shear and greater chaotic contact between cellulose particles and oxygen, which facilitated the generation of more negative charges on the surface of cellulose crystals due to the partial rupture of the particles [46].

In Fig. 1d, the chemical shifts of the C atoms were C1 (102 ppm), C4 (87.1 ppm), C4 (84.3 ppm), C2/C3/C5 (74.3/73.6/71.9 ppm), C61 (64.5 ppm) and C62 (60.7 ppm) [47]. These results showed that the type I structure of cellulose still existed after alkylation modification. Compared with PCNCs, KH-550 with alkylation modification increased the intensity of the signal peak of $-CH_2-NH_2$ on KH-550 at 41.2 ppm. The peak at C235 for the sample with a sonication time of 3 h in Fig. 1d was the same as that of the PCNC without sonication modification, which may be due to the fact that the high sonication energy over a long period destroyed the structure of the CNCs and affects the DS. According to the DS and WCA, the ultrasonic treatment time was 2 h for the next ultrasonic treatment power analysis.

As shown in Fig. 1e, with the increase of ultrasonic treatment power, the WCA and DS of K-PCNCs first increased and then decreased. When the ultrasonic treatment power was 450 W, the WCA and DS reached the highest values of 135° and 1.53°, respectively.

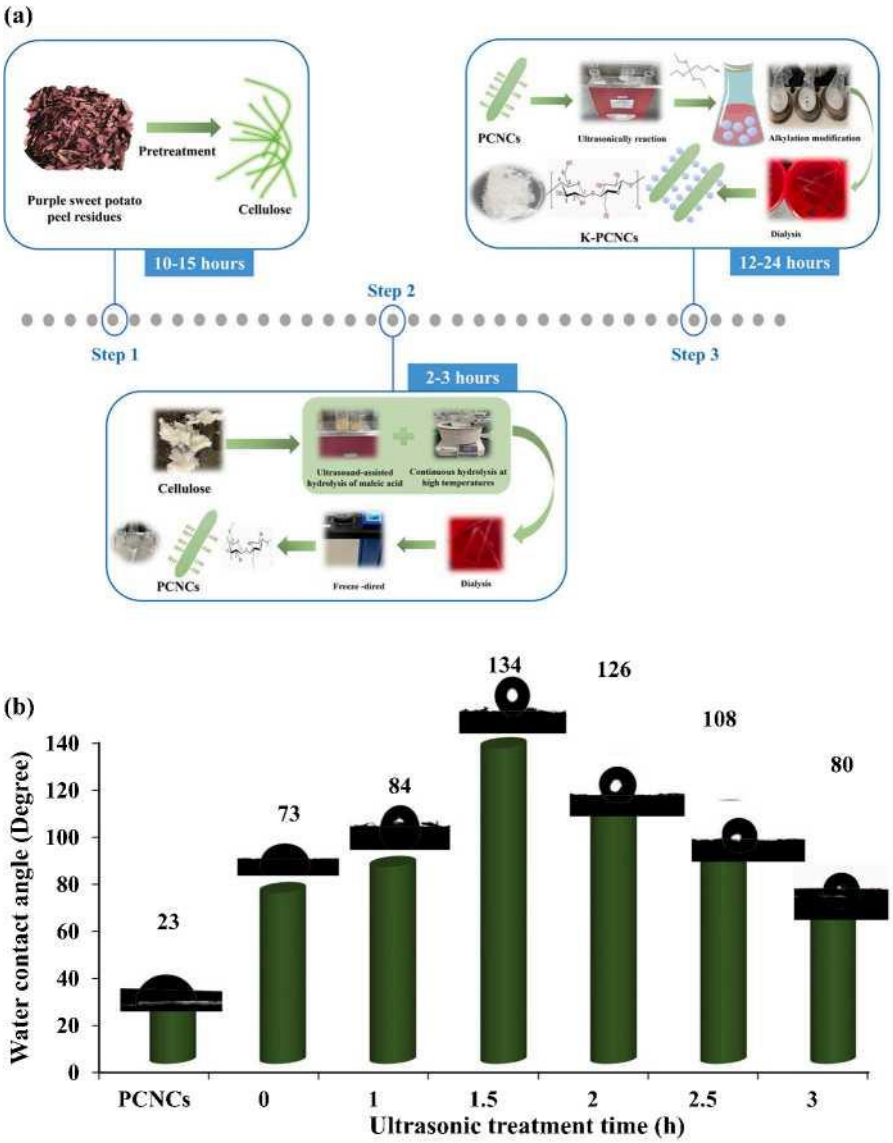

Fig. 1. Effect of different ultrasonic treatment times and power on WCA and DS of K-PCNCs. The modification routes of PCNCs (R refers to the grafted groups or H according to the degree of substitution) (a), water contact angle analysis (b), degree of substitution (c), and NMR (d) analysis of K-PCNCs prepared at different ultrasonic treatment times (power: 450 W), water contact angle analysis (e), degree of substitution (f) and NMR (g) analysis of K-PCNCs prepared at different ultrasonic treatment power (time: 2 h). Abbreviations in the figure are as follows: PCNCs (purple sweet potato peel residue CNCs), K-PCNCs (alkylated purple sweet potato peel residue CNCs). Different letters (a-f) indicate significant differences between values ($p < 0.05$).

When the ultrasonic treatment power was >450 W, the WCA and DS decreased. Like different ultrasonic treatment time-assisted alkylation modifications, K-PCNCs still retained the cellulose type I structure in the process of different ultrasonic power-assisted alkylation modifications, that is, different ultrasonic treatment power did not change the chemical structure of PCNCs. Fig. 1g showed that the intensity of the cellulose characteristic peaks in the ^{13}C NMR spectrum, especially the condensation peaks belonging to C2, 3, 5, and C6, decreased at the same time, showed that sialylation occurs not only on the expected hydroxyl groups of C6 but also on the hydroxyl groups of C2 and C3 [48]. The results showed that the ultrasonic treatment time of 2 h and ultrasonic treatment power of 450 W were the best ultrasonic treatment conditions for ultrasonic-assisted alkylation modification. The optimum DS and WCA of K- PCNCs were 1.53 and 135°, respectively. Proper ultrasonic-assisted alkylation hydrolysis has significantly improved the hydrophobicity of K-PCNCs.

PHYSIOCHEMICAL, STRUCTURAL PROPERTIES, AND THERMAL PERFORMANCE ANALYSIS OF K-PCNCS

As shown in Fig. 2a, compared with PCNCs (-45.8 ± 0.2 mV), the value of zeta potential of K-PCNCs (-42.6 ± 0.9 mV) and K-PCNCs (U) (-40.8 ± 0.6 mV) decreased after alkylation modification. Compared with K-PCNCs modified by ultrasound, the absolute value of zeta potential without ultrasound was significantly lower, indicating that ultrasound-assisted modification can significantly improve colloidal stability [49]. K-PCNCs were freeze-dried and redispersed in different solvents, such as water, ethanol, and toluene (0.2 %). Photographs of these suspensions were shown in Fig. 2b. Compared with K-PCNCs (U), K-PCNCs prepared under the best ultrasonic treatment conditions have a good affinity for ethanol (3) and can form a stable suspension. K-PCNCs showed greater dispersion in absolute ethanol and higher particle stability and were well dispersed in toluene and the formation of some flocs at the bottom, indicating that ultrasound can improve the stability of the suspension. Alkylation of PCNCs significantly improved the colloidal dispersibility in different solvents and improved the application value.

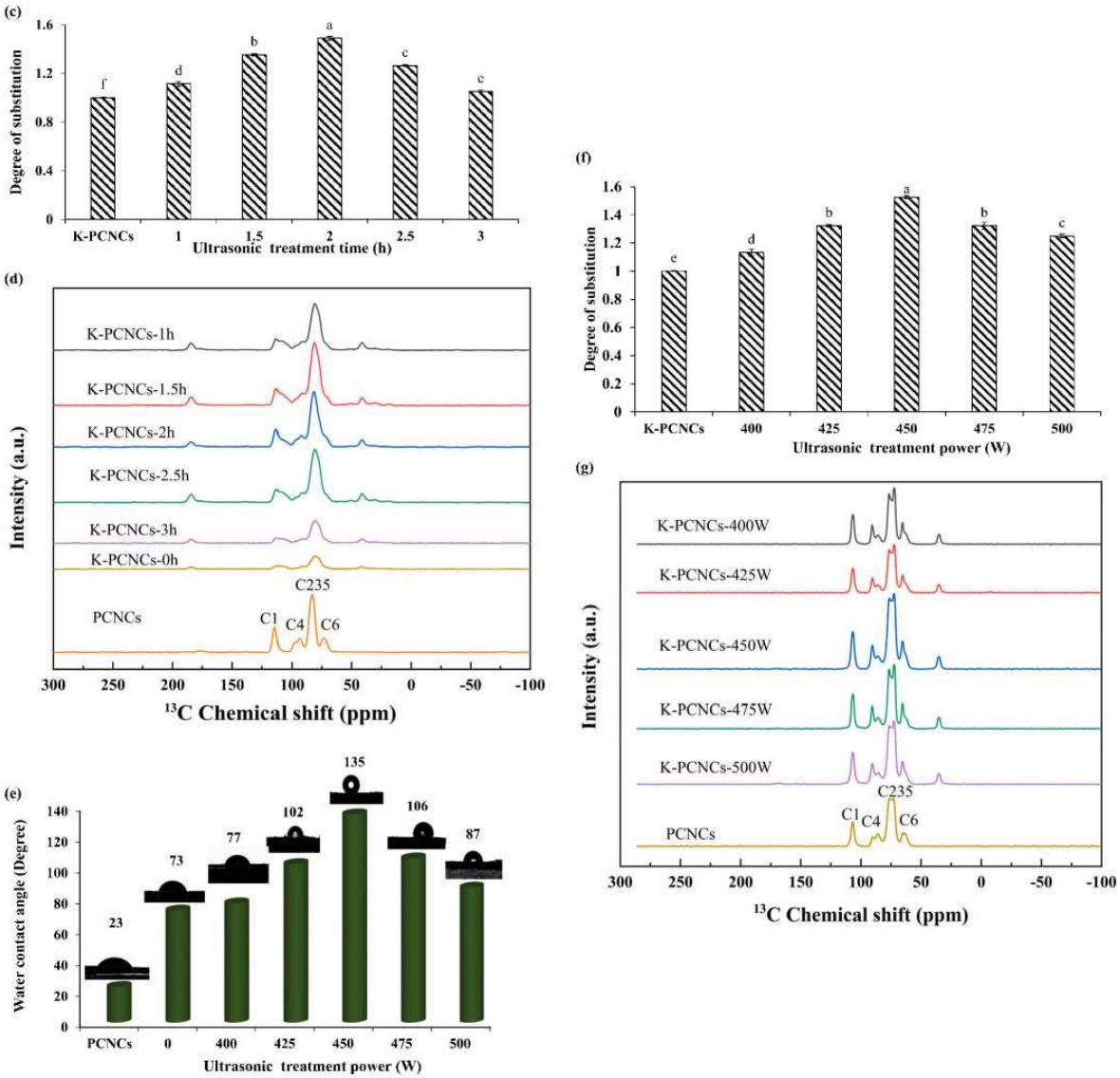

Fig. 1. (*continued*).

Fig. 2c showed the AFM diagram of K-PCNCs. The diameter range of K-PCNCs was 27-35 nm and the length range was 100-260 nm (Fig. 2f and h). The diameter range of PCNCs was 10-30 nm, and the length range was 60-220 nm. K-PCNCs typically exhibited rod-like structures, like the PCNCs. In TEM analyses (Fig. 2d), the K-

PCNCs appeared relatively uniform structures. The highly modified CNCs crystals played a major role in the application potential of this nanomaterial. Moreover, because of the erosion and swelling effect, the blurry outline of K-PCNCs led to a larger diameter [50]. In general, after chemical modification, CNCs maintained the original rod shape.

Fig. 3a showed that there was an absorption peak at 3350 cm^{-1}, which was the stretching vibration of the OH group in cellulose molecule, 1620 cm^{-1} represented the bending vibration of O-H, and 1065 cm^{-1} represented the stretching vibration of C-O. The absorption peaks at 2900 cm^{-1} and 896 cm^{-1} were due to the C-H group and the p-glycosidic bond, respectively [51]. These peaks became broader and more complex as the siloxane chains became more branched. Compared with PCNCs, the characteristic peak of amino groups (-H2N) in K-PCNCs appeared at 1600 cm^{-1}, which was related to strong hydrogen bonding to the hydroxyl groups with both silanol and cellulose [52]. In addition, there were also some slight shifts in the peaks at 1164 and 1030 cm^{-1} for PCNCs to 1157 and 1023 cm^{-1} in K-PCNCs, respectively. The analysis of FTIR data showed that 1745 cm^{-1} represents the C=O stretching vibration of hemicellulose, and 1506 cm^{-1} represents the C=O telescoping vibration of lignin and the benzene ring backbone vibration [53]. The absence of such characteristic peaks in the PCNCs and K- PCNCs spectra indicated that the lignin and hemicellulose were both removed, which can be further used as biomaterials. The reaction on the surface of ultrasound-assisted alkylated CNCs produced alkylsubstituted CNCs.

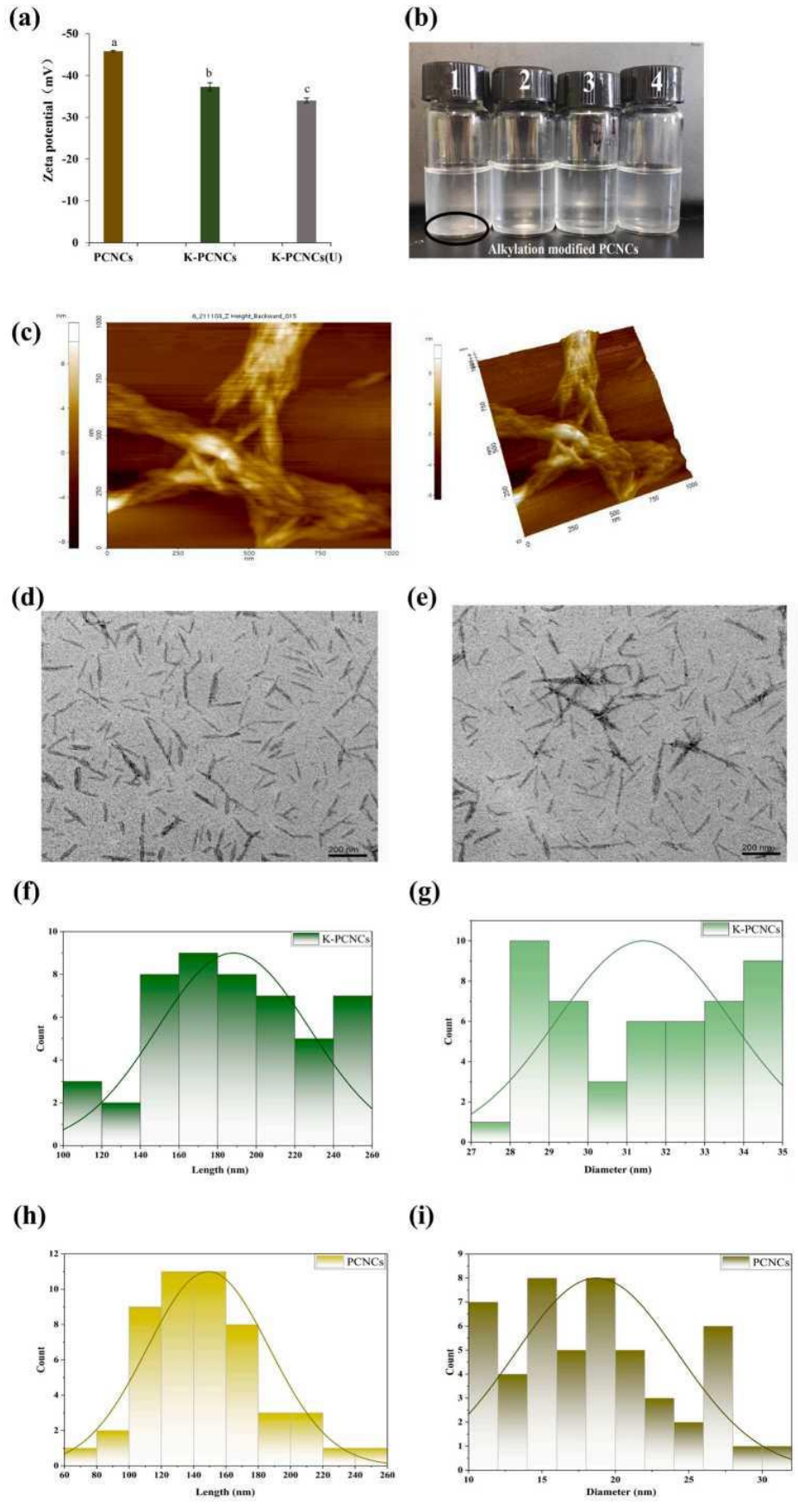

(caption on next page)

Fig. 2. Dispersibility, morphological properties, and dimensional characterization of K-PCNCs and PCNCs. Zeta potential of K-PCNCs and K-PCNCs (U) (a), dispersion of K-PCNCs (b), AFM analysis (c) of K-PCNCs, TEM analysis of K-PCNCs (d) and PCNCs (e), length (f, h) and diameter (g, i) distributions of PCNCs and K-PCNCs. Abbreviations in the figure are as follows: PCNCs (purple sweet potato peel residue CNCs), K-PCNCs (alkylated purple sweet potato peel residue CNCs), K-PCNCs (U) (alkylated purple sweet potato peel residue CNCs prepared without ultrasonic condition). 1, 2, 3, and 4 represent the dispersibility of K-PCNCs in the control group without ultrasonic conditions, aqueous solution, absolute ethanol, and toluene dispersant. Different letters (a-c) indicate significant differences between values ($p < 0.05$).

During the highly modified alkylation process, the cellulose I structure of CNCs was retained, as evidenced by XRD analysis of K-PCNCs (Fig. 3b). The XRD indicated that the substitution of alkyl groups preserves the core crystalline structure of cellulose. The intensities of diffraction peak in 2θ = 15.4° and 22.7° corresponded to the CNCs crystal surfaces at (110) and (200) were significantly enhanced, and the crystallinity of K-PCNCs (65.4 ± 4.2°) significantly increased after modification. Compared with previous studies, the crystallinity of K- PCNCs was higher than that of salinization-modified CNCs (43.8 ± 0.9 %) [31], showing its potential as a reinforcing component for composites. This indicated that the crystal shape and main crystal structure did not change during the modification process, and the crystallinity was enhanced. Fig. 3c showed that the chemical bond types of the macromolecules on the surface of K-PCNCs existed, all of which are C1 (C-C/C- H), C2 (C-OH), and C3 (C=O). The C—C content of K-PCNCs gradually increased, while the C=OH content gradually decreased. After modification, fewer hydroxyl groups were exposed on the surface of K-PCNCs. The XPS spectrum of O1s indicates (Fig. 3e) that oxygen and carbon atoms were mainly connected through C—O bonds. The peaks in the O1s spectrum of XPS were fitted into two peaks, O1s1 (C-OH...O) and O1s2 (C-OH) [54]. The proportion of O1s2 in K-PCNCs gradually decreased, indicating a decrease in the proportion of free hydroxyl groups without hydrogen bonds and a decrease in surface hydroxyl content. This showed that a chemical reaction has occurred between the alkyl group and the hydroxyl groups on the surface of CNCs, completed the alkylation modification and further aligned with the NMR results.

Fig. 3g showed the DSC patterns of PCNCs and K-PCNCs. The DSC baseline responded to the change in the heat capacity of the substance, and the change in the baseline was caused by the change in the molecular structure of the sample and the structure of the aggregation state. The heat absorption degradation temperature of PCNCs was decreased compared with K-PCNCs, because of the decreased in polymerization, decreased particle size, so the terminal carbon and exposed reactive groups on the surface were significantly increased and the thermal stability was increased [55]. In contrast, there was no difference in the absorption decomposition temperature of the DSC secondary heating curves of K-PCNCs, which have good thermal properties. Thermal analyses of PCNCs and K-PCNCs revealed different degradation profiles (Fig. 3h). The initially small weight loss of K-PCNCs of 100—150 °C can be attributed to the evaporation of physically bound moisture [56]. The main peaks corresponding to the thermal degradation of K-PCNCs were observed between 240 and 280 °C, and a small wide dip (310 and 450 °C). K-PCNCs lost nearly 30 % of the mass in the 250 °C range, followed by another 45 % mass loss at temperatures (300—500 °C), lead a significantly high (nearly 20 %) residue at 500 °C. The decomposition temperature range of PCNCs was 210—395 °C, and the weight loss was 86 %. The onset degradation temperatures (T_{onset}) of K-PCNCs were 340.81 °C. The maximum degradation temperature (T_{max}) was 424.57 °C (Fig. 3j). The weight loss of K-PCNCs was 79 %. The crystalline zone that was difficult to be intruded will at the same time lead to an increase in thermal stability, a result that was consistent with previous XRD studies. Similar results also appeared in the study of Wang et al. (2024) [57] that the maximum DTG peak of the prepared tea- derived CNCs was 273 °C. A shoulder peak at 229 °C preceded the central decomposition peak of the tea-derived CNCs. This stage of degradation is consistent with that reported by Roman et al. (2004) [58]. The multiple thermal degradation peaks in the curve of K-PCNCs because, during the process of thermal degradation, the surface-grafted long-chain polymers preferentially degraded to produce thermal crossproducts [59]. The thermal stability of K-PCNCs was significantly improved compared to PCNCs. K-PCNCs have a major thermal degradation temperature above 200 °C and can be used as reinforcing materials in green bio composites.

PREPARATION AND CHARACTERIZATION OF HA SYNTHESIZED WITH K-PCNCS AS A DISPERSANT

The mechanism of forming a three-dimensional porous scaffold for bone defect repair was shown in Fig. 4. Firstly, CNCs were prepared from purple sweet potato peel residues and modified by alkylation-assisted ultrasonication modification. Then, modified CNCs were used as dispersants for HA prepared by chemical synthesis to improve the agglomeration of HA. The prepared HA has a nanostructure. It was compounded with PVA, frozen in liquid, and transferred to a vacuum freeze-drying device. During the vacuum freeze-drying process, as the solvent evaporated, the volume of water decreased, and pores uniformly appeared in the scaffold. Finally, the porous structures were interconnected and formed through holes. During the solvent evaporation process, the hydrogen bonding forced and the bonding between HA tightly adhered to the porous scaffold, thereby forming a uniform through-hole structure during the water drying process. The porous scaffold bound and adsorbed osteoblasts on the pore site, allowed the cell to proliferate, differentiate, and repair bone defects during the mineralization process of osteoblasts.

Interactions between HA and K-PCNCs were observed by TEM (Fig. 5). HC-K particles with a length of 200 nm and a width of 40—50 nm were observed in the TEM image. In the presence of calcium hydroxide and phosphoric acid, HA formed spherical particles modified in the rodlike structure of K-PCNCs [39]. This result was like the size of HAP observed in the study of Shuai et al. (2022), the HAP powders were needle-like with a length of about 150 nm and a width of about 20 nm, suggesting that the synthesis of HA particles in modified CNCs did not alter the morphological size of HA [60]. This interaction was also attributed to the formation of hydrogen bonds between the OH group of nano dispersants and the Ca^{2+} of HA [61]. The synthesis of HC-K in the suspension of K-PCNCs demonstrated the modification of HA along the rod-like structure of CNCs.

CA/P RATIO ANALYSIS OF HA

To determine the Ca/P ratio of HA, the EDS spectra of the HA particles were shown in Table 1. The HA synthesized with K-PCNCs, PCNCs, and CCNCs as dispersants has the same elemental composition consisting of four elements, from calcium carbonate and phosphorus, which was the same as that of HA particles (Fig. 6). HC-K with a Ca/P ratio of 1.60, that was in the range of biological apatite from 1.50 to 1.85. The Ca/P ratio of natural HA was 1.67, while sono chemical-prepared HA/ cellulose composites ranged from 1.78 to 1.90 and 1.40—1.60 prepared by simulated body fluids [62—65], which indicated that the HA synthesized with K-PCNCs as a dispersant was closer to the standard stoichiometric ratio than that of the other methods, suggested that ultrasound-assisted modification has a significant influence on the CNCs dispersants.

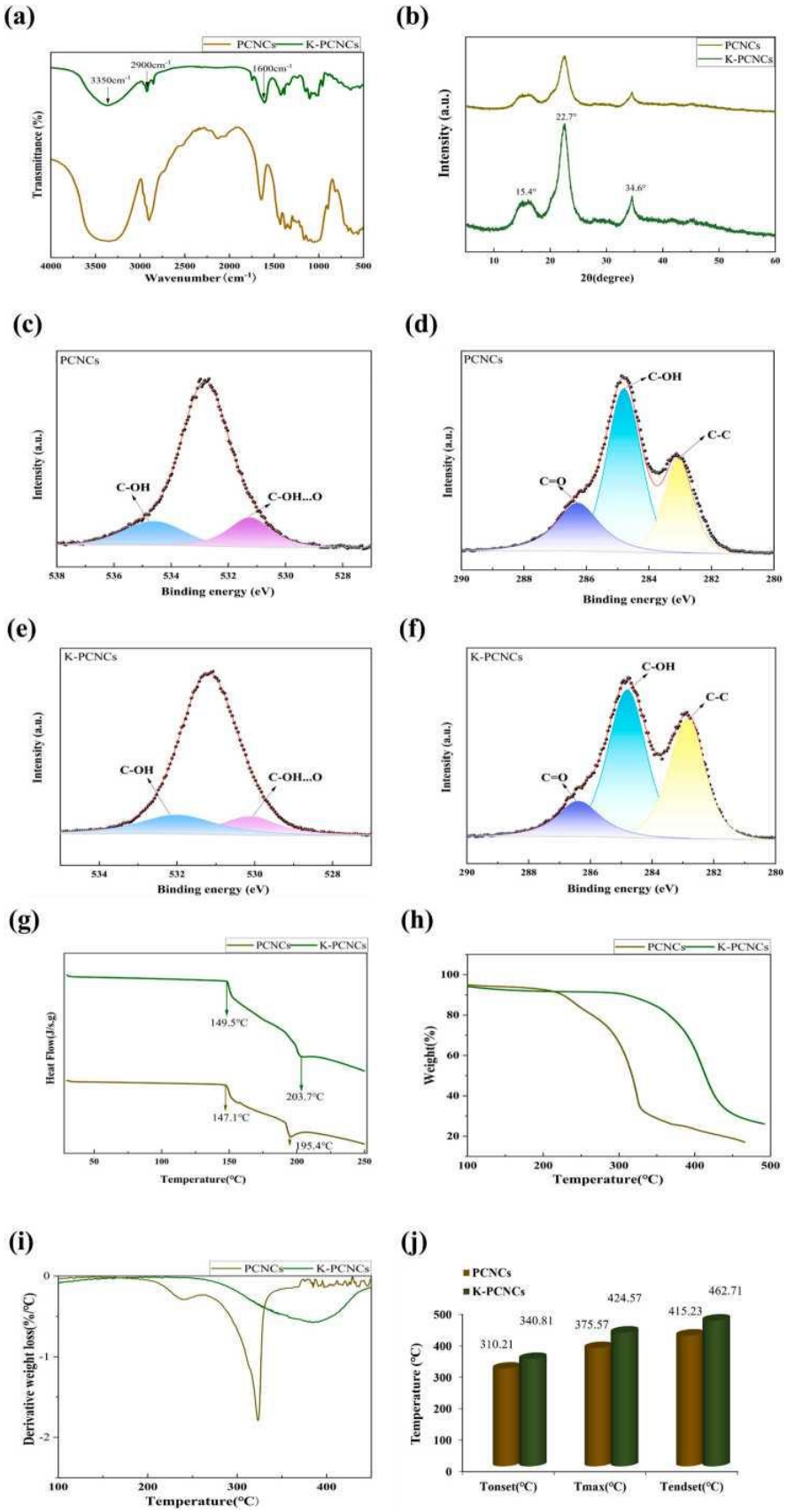

(caption on next page)

Fig. 3. Structural properties and thermal characterization of K-PCNCs and PCNCs. FTIR (a), DSC (b), TGA (c), and DTG (d) analysis of PCNCs and K-PCNCs, the onset degradation temperature-Tonset, the maximum degradation temperature-Tmax, and the end degradation temperature-Tendset of K-PCNCs and PCNCs (e), XRD (f), and XPS elemental carbon (g, i) and oxygen (h, j) analysis of PCNCs and K-PCNCs. Abbreviations in the figure are as follows: PCNCs (purple sweet potato peel residue CNCs), and K-PCNCs (alkylated purple sweet potato peel residue CNCs).

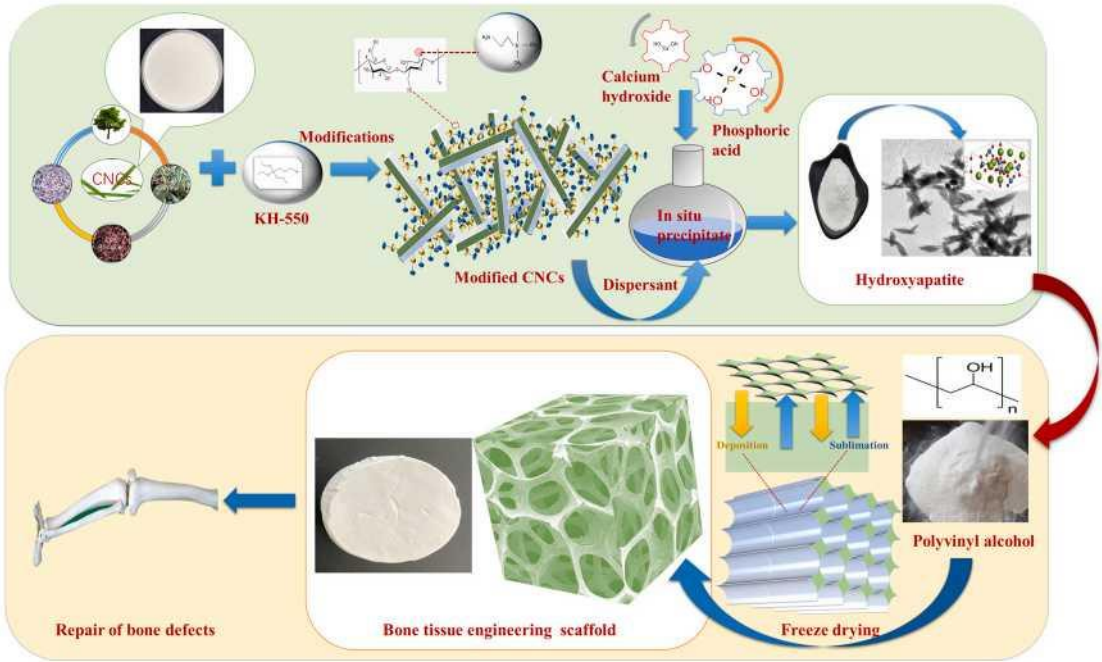

Fig. 4. Diagram of the mechanism underlying the formation of the bone tissue engineering scaffold.

MORPHOLOGICAL STUDY, POROSITY, AND SWELLING BEHAVIOR OF HA BONE TISSUE ENGINEERING SCAFFOLDS

The effect of change in the HA addition on the morphology of the bone tissue engineering scaffold can be seen through the microstructure changes by SEM (Fig. 7). The structure of bone tissue engineering scaffolds promoted cell biological reactions and microenvironment, thus promoting cell proliferation. The ice template method was used to synthesize the scaffolds. The microporous structure of the scaffold was preserved by freeze-dried ice sublimation. Fig. 7 showed that all the bone tissue engineering scaffolds successfully prepared by ice template technology had a highly interconnected 3D structure of pore channels and pore matrix. SEM showed that the porosity and homogeneity of the PHC-HA scaffolds prepared with HA synthesized without CNCs as a dispersant were significantly lower than those of the scaffolds prepared with HA synthesized with modified CNCs as a dispersant. Among the bone tissue engineering scaffolds prepared with HA synthesized with K- PCNCs, PCNCs, and CCNCs as dispersants, the scaffolds prepared with HA synthesized with K-PCNCs as dispersants had relatively high porosity and equilibrium swelling rate, and relatively uniform porosity. Table 2 showed that the bone tissue engineering scaffolds prepared with 3, 6, 9, and 12 % HA addition had the highest porosity and equilibrium swelling rate when 9 % HA was added (56.1 % and 807.7 %, respectively). There was good uniformity between PVA and HA particles, and there was no free HA aggregation in the internal porous structure of the scaffold. For the combination of PVA and different amounts of HA, the internal space of the bone tissue engineering scaffold had different degrees of influence, showing different porous structures. This proved that HA synthesized by different dispersants directly affected the internal structure of the scaffold as the skeleton part of the bone scaffold [40].

FTIR, XRD, MECHANICAL PROPERTIES, AND WCA ANALYSIS OF BONE TISSUE ENGINEERING SCAFFOLDS

Fig. 8(a, b, c, d) showed that the changes in functional groups during the synthesis of the scaffolds were characterized by infrared spectroscopy. The combination of HA and PVA resulted in hydrogen interactions; thus, the amount of chemical functional groups grafted on the scaffold changes, which further changes the peak strength of the different scaffolds in the FTIR spectrum. The FTIR spectra of the PVA and scaffolds (3, 6, 9, 12 %) showed characteristic peaks at 3430 cm^{-1} (-OH), 2900 cm^{-1} (CH_2), 1430 cm^{-1} (CH), 918 cm^{-1} (C—O) and 845 cm^{-1} (C—C), indicated the existence of cellulose and PVA. The characteristic peaks at 1035, 682, 601, and 536 cm^{-1} represented the different vibration modes of phosphate groups (PO^{4}_{3}) in HA. Specifically, 1035 cm^{-1} was attributed to the asymmetric tensile mode of phosphate, while the O-P-O mode corresponded to the peaks at 682, 601, and 536 cm^{-1} [66]. The appearance of these characteristic peaks represented HA confirmed the existence of HA in bone tissue engineering scaffolds. When the amount of HA increased, the intensity of the phosphate (PO^{4}_{3}) peak increased. The interaction of the -OH group in HA and Ca^{2+} in the PVA scaffold reduced the unbound -OH group in the bone tissue engineering scaffold, resulted in a decrease in the band strength at 3430 cm^{-1}. The HO- group to Ca^{2+} hydrogen bond connected in bone tissue engineering scaffold affects other physical properties of the scaffold.

The crystallization behavior of the bone tissue engineering scaffold was characterized by XRD. The hydrogen interaction between HA and PVA destroyed the crystallinity of the scaffolds. Fig. 8(e, f, g, h) showed that the peaks at 2θ = 19.4° and 40.1° represented the crystallization region of PVA. 2θ = 22.5° (200), 25.7° (002), 31.6° (210), 32.6° (211), 34.0°, and 40.1° (310), and 46.5° (222) corresponded to CNCs and HA. The peak distribution agreed with the study of Shuai et al. (2022) [67]. Also, the diffraction peak results indicated that the obtained HA particles were nano-microcrystalline and were considered to have excellent osseointegration properties [68]. At 2θ = 19.4° for PVA, as the amount of HA increased, the strength of the main peak gradually decreased, resulting in a decrease in crystallinity, indicating that the connection between the HO group and Ca^{2+} hydrogen bonds through the interaction of -OH groups destroyed the natural crystallization

region of PVA [9]. The HA graft changed the number and order of the hydroxyl functional groups in the different CNCs dispersants, resulting in the customized synthesis of the internal porous structure of the prepared scaffolds. The amount of HA was related to the decrease in crystallinity in scaffolds. The physicochemical performance and internal structure of HA and PVA increased the compressive modulus of interconnected bone tissue scaffolds under pressure, further enhancing mechanical performance. The WCAs of the PVA, PHC-K9, and PHC-P9 scaffolds were 53 ± 5°, 113 ± 4°, and 50 ± 4°, respectively, indicated that the scaffolds had good hydrophobicity (Fig. 8i). The physiochemical properties and morphological analysis showed that the PHC-K9 bone tissue engineering scaffold has good biocompatibility.

A compression experiment was used to show the trend of changes in the mechanical properties of the bone tissue engineering scaffold. The relationship between the type and amount of HA and the compression modulus was shown in Fig. 8j. Although HA reduced the crystallinity of PVA and destroyed its original crystal structure, as the amount of HA added increased, the compression modulus gradually increased, indicated that HA also helps to improve the mechanical resistance of bone scaffolds. When the content of HA was 9 %, the mechanical properties of the scaffold prepared with K-PCNCs as dispersant reached the maximum value (0.085 ± 0.004 MPa). The compression modulus of PHC-K9 was approximately 286.4 % higher than that of PVA. The increase in the load of K-PCNCs and HA particles in the scaffold strengthened the interior of the porous structure and improved the mechanical strength of the whole scaffold, which confirmed the enhanced mechanical properties due to the increase in the solid content [69].

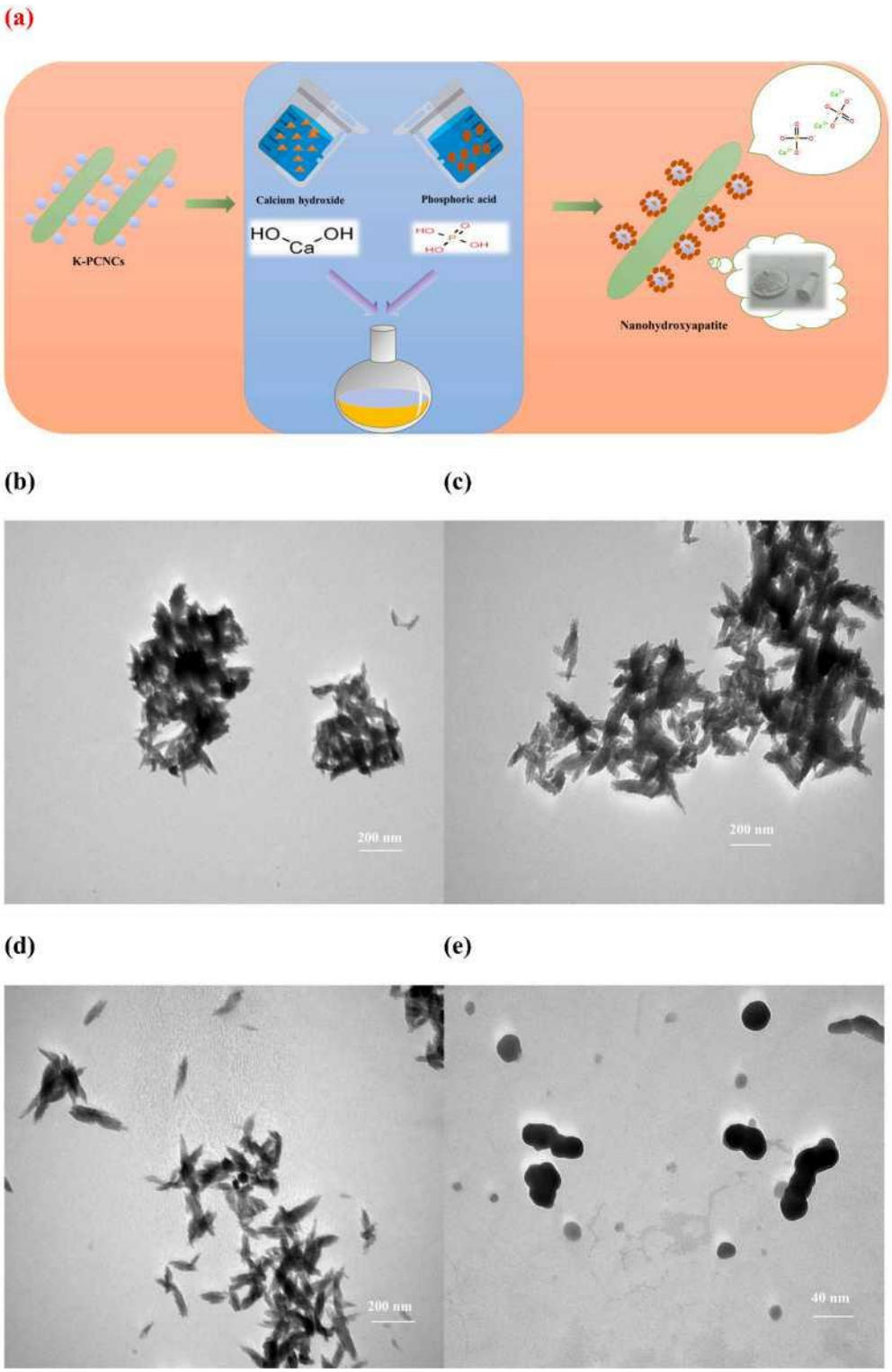

Fig. 5. Diagram of the formation mechanism of the hydroxyapatite (a), TEM analysis of HC-K (b), HC-C (c), HC-P (d), HA (e), and flow chart of hydroxyapatite preparation (f). Abbreviations in the figure are as follows: HA (commercial hydroxyapatite), HC-C (hydroxyapatite synthesized with CCNCs as a dispersant); HC-K (hydroxyapatite synthesized with K-PCNCs as a dispersant), HC-P (hydroxyapatite synthesized with PCNCs as a dispersant).

Table 1. *Ca/P ratio of the hydroxyapatite.*

Samples	Atomic percentage of elements (%)				Ca/P
	C	O	Ca	P	
HA	51.98 ± 0.30^{c}	40.73 ± 0.20^{b}	4.67 ± 0.02^{b}	2.33 ± 0.01^{c}	2.00 ± 0.00
HC-C	53.17 ± 0.15^{b}	39.15 ± 0.10^{c}	5.29 ± 0.01^{a}	2.39 ± 0.03^{b}	2.21 ± 0.02
HC-P	54.52 ± 0.22^{a}	40.50 ± 0.19^{b}	3.68 ± 0.00^{d}	1.30 ± 0.02^{d}	2.83 ± 0.04
HC-K	48.26 ± 0.25^{d}	44.27 ± 0.10^{a}	4.60 ± 0.00c	2.87 ± 0.01^{a}	1.60 ± 0.00

Abbreviations in the table are as follows: HA (commercial hydroxyapatite), HC-C (hydroxyapatite synthesized with CCNCs as a dispersant), HC-K (hydroxyapatite synthesized with K-PCNCs as a dispersant), HC-P (hydroxyapatite synthesized with PCNCs as a dispersant). Different letters (a-d) indicate significant differences between values ($p < 0.05$).

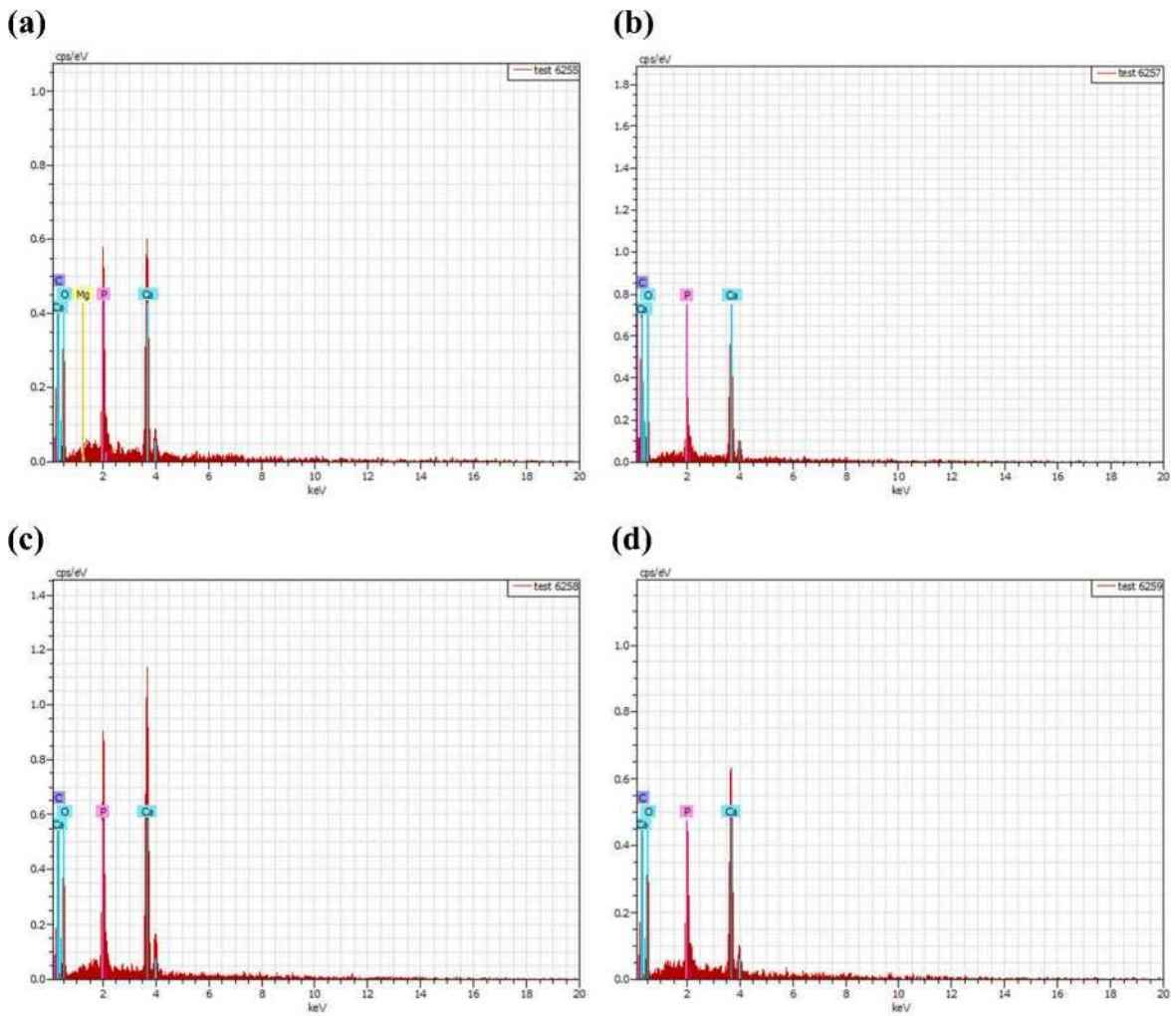

Fig. 6. EDS analysis of hydroxyapatite particles. (a) HC-K, (b) HC-C, (c) HC-P, (d) HA. Abbreviations in the figure are as follows: HA (commercial hydroxyapatite), HC-C (hydroxyapatite synthesized with CCNCs as a dispersant), HC-K (hydroxyapatite synthesized with K-PCNCs as a dispersant), HC-P (hydroxyapatite synthesized with PCNCs as a dispersant.

(a)

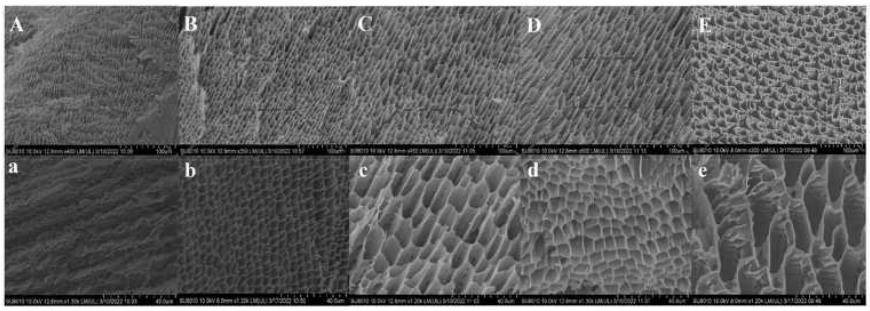

(b)

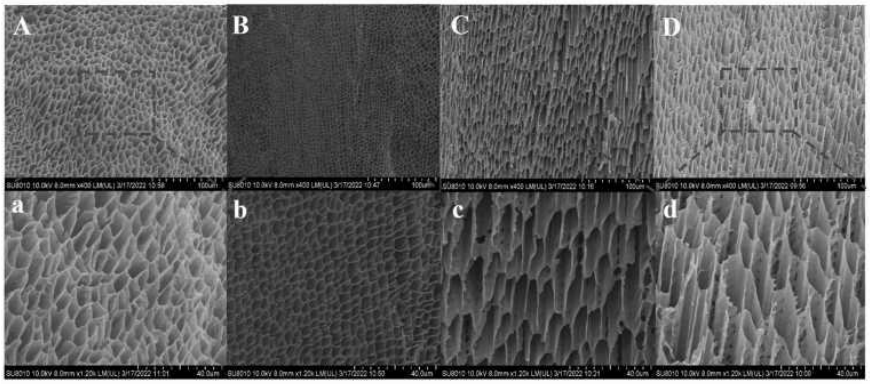

(c)

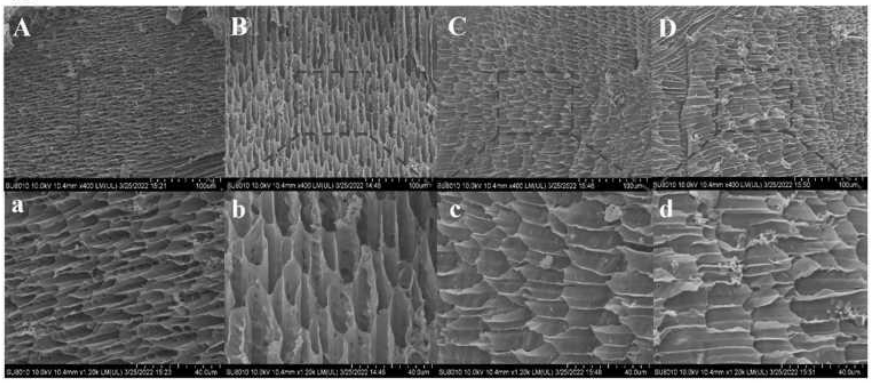

(d)

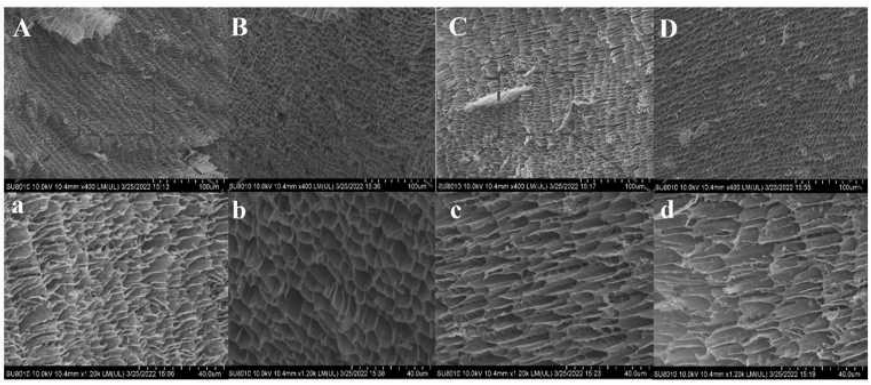

(caption on next page)

Fig. 7. SEM of PHC-K composite scaffolds (a) (**A** and **a**: PVA, **B** and **b**: PHC-K3, **C** and **c**: PHC-K6, **D** and **d**: PHC-K9, **E** and **e**: PHC-K12, **A/B/C/D/E**: 1200x, scalebar: 100 µm, **a/b/c/d/e**: 400x, scalebar: 40 µm), PHC-C composite scaffolds (b) (**A** and **a**: PHC-C3, **B** and **b**: PHC-C6, **C** and **c**: PHC-C9, **D** and **d**: PHC-C12, **A/B/C/D**: 1200x, scalebar: 100 µm, **a/b/c/d**: 400x, scalebar: 40 µm), PHC-P composite scaffolds (c) (**A** and **a**: PHC-P3, **B** and **b**: PHC-P6, **C** and **c**: PHC-P9, **D** and **d**: PHC-P12, **A/B/C/D**: 1200x, scalebar: 100 µm, **a/b/c/d**: 400x, scalebar: 40 µm), and PHC-HA composite scaffolds (**A** and **a**: PHC-HA3, **B** and **b**: PHC-HA6, **C** and **c**: PHC-HA9, **D** and **d**: PHC-HA12, **A/B/C/D**: 1200x, scalebar: 100 µm, **a/b/c/d**: 400x, scalebar: 40 µm). Abbreviations in the figure are as follows: PVA (polyvinyl alcohol scaffold), PHC-K (hydroxyapatite synthesized with K-PCNCs as a dispersant/polyvinyl alcohol composite scaffolds), PHC-C (hydroxyapatite synthesized with CCNCs as a dispersant/polyvinyl alcohol composite scaffolds), PHC-P (hydroxyapatite synthesized with PCNCs as a dispersant/polyvinyl alcohol composite scaffolds), PHC- HA (commercial hydroxyapatite/polyvinyl alcohol composite scaffolds). 3, 6, 9, and 12 % were the addition amounts of the hydroxyapatite in the composite scaffolds.

Table 2

Samples	Pore size (μm)	Porosity (%)	Equilibrium swelling rate (%)
PVA	43.7 ± 6.4^{f}	50.9 ± 1.2^{h}	612.7 ± 13.6^{e}
PHC-K3	71.9 ± 7.8^{bcdef}	53.1 ± 0.13^{bcdefgh}	730.1 ± 11.3^{abcde}
PHC-K6	92.7 ± 6.4^{abcde}	55.2 ± 0.4^{bcde}	785.6 ± 76.8^{abcd}
PHC-K9	102.9 ± 6.7^{ab}	56.1 ± 3.1^{abc}	807.7 ± 89.8^{abc}
PHC-K12	108.2 ± 11.9^{a}	58.9 ± 0.2^{a}	822.8 ± 15.3^{a}
PHC-C3	69.0 ± 8.5^{gh}	51.0 ± 1.4^{gh}	664.1 ± 50.7^{de}
PHC-C6	85.5 ± 12.0^{abcde}	53.6 ± 0.2^{bcdefgh}	706.0 ± 56.4^{abcde}
PHC-C9	97.5 ± 10.6a^{bcde}	54.7 ± 3.3^{bcdef}	737.7 ± 18.2a^{bcd}
PHC-C12	96 ± 8.5^{abcde}	55.8 ± 0.4^{abcd}	750.3 ± 39.4^{abcd}
PHC-P3	66.5 ± 9.2^{def}	51.9 ± 0.4^{efgh}	662.9 ± 78.1d^{e}
PHC-P6	82.5 ± 7.7^{abcde}	53.8 ± 1.7^{bcdefgh}	713.7 ± 61.4^{abcde}
PHC-P9	93.0 ± 7.1^{bcdefgh}	54.3 ± 1.7^{bcdefgh}	750.5 ± 45.0ab^{cd}
PHC-P12	101.0 ± 5.6^{abc}	55.0 ± 1.7^{bcde}	762.8 ± 44.1^{abcd}
PHC-HA3	65.0 ± 7.1^{ef}	51.3 ± 1.8^{fgh}	695.9 ± 52.8^{cde}
PHC-HA6	71.0 ± 4.2^{cdef}	52.2 ± 1.0^{defgh}	755.1 ± 28.1^{abcd}
PHC-HA9	79.5 ± 9.1a^{bcde}	52.5 ± 0.2^{cdefgh}	710.9 ± 56.5^{abcde}
PHC-HA12	84.0 ± 8.5^{abcde}	53.1 ± 0.3^{bcdefgh}	743.0 ± 18.4^{abcd}

Abbreviations in the table are as follows: PVA (polyvinyl alcohol scaffold), PHC- K (hydroxyapatite synthesized with K-PCNCs as a dispersant/polyvinyl alcohol composite scaffolds), PHC-C (hydroxyapatite synthesized with CCNCs as a dispersant/polyvinyl alcohol composite scaffolds), PHC-P (hydroxyapatite synthesized with PCNCs as a dispersant/polyvinyl alcohol composite scaffolds), PHC-HA (commercial hydroxyapatite/polyvinyl alcohol composite scaffolds). 3, 6, 9, and 12 % were the addition amounts of the hydroxyapatite in the composite scaffolds. Different letters (a-h) indicate significant differences between values ($p < 0.05$).

The mechanical strength of the bone tissue engineering scaffold prepared with modified CNCs as a dispersant was significantly greater than that of the prepared with unmodified CNCs as a dispersant, which proved the importance of modified CNCs as the biological dispersant for bone scaffolds.

CYTOTOXICITY, CELL VIABILITY, AND IN VITRO DEGRADATION OF BONE TISSUE ENGINEERING SCAFFOLDS

According to the results of equilibrium swelling rate, porosity, and pore size in Table 2 and the mechanical properties in Fig. 8j, PHC-K9 scaffolds have good properties, so the scaffold for the biocompatibility study while PVA and PHC-P9 were used as a control for comparative analysis. PHC-K9 was selected for cell studies while PVA and PHC-P9 were used as controls. In vitro degradation tests were to evaluate the effect of the degradation rate of the scaffolds (Fig. 9a and b). The weight loss for PVA scaffolds was 2.34 % (w/w), almost doubled for PHC-P9 (2.90

%, w/w) and tripled for PHC-K9 (4.07 % w/w) after a 1-month degradation in 10 % H2O2. After 30 days of incubation in PBS (Fig. 9b), the degradation loss of the PVA scaffolds was 20 %-22 %, that of the PHC-P9 scaffolds was around 23-24 %, and that of the PHC-K9 scaffolds was around 25 %, a result like the degradation rate of the HA-composite gelatin scaffolds prepared by Morsy et al. 2024 (after 35 days of incubation in PBS of 20-25 %) [43]. Therefore, CNCs enhanced the diffusivity of the water molecules in the biocomposite matrix. The degradation curves of the scaffolds could confirm the cross-linking efficiency as well as the suitability to meet bone tissue engineering conditions. In bone tissues, the rapid degradation of a scaffold may lead to poor mechanical strength and low stiffness and thus can negatively influence bone regeneration [70].

The cytotoxicity of the PVA, PHC-K9, and PHC-P9 scaffolds was evaluated by measuring the cell viability of the MC3T3-E1 osteoblasts cell cultured for 24 h. Fig. 9a showed that the scaffold has no toxic effect on osteoblasts. The cell viability was approximately 90 % greater in the three scaffold groups. A cell viability value above 80 % indicated no cell cytotoxicity [71]. Fig. 9c showed that PHC-K9 (98.02 ± 0.84 %) and PHC-P9 (93.02 ± 6.47 %) had similar cell survival rates. The PVA led to a slightly lower percentage of viable cells (0.25 ± 2.62 %). This was adequate for demonstrating the safe use of the scaffolds on cells. The bone tissue engineering scaffolds were prepared from PVA, and HC without cytotoxicity; at the same time, interconnected pore structures can promote cell extension, thereby promoting proliferation and differentiation.

To quantitatively test the biocompatibility of the scaffolds, the viability of MC3T3-E1cells cultured on the PHC-K9, PHC-P9, and PVA scaffolds was evaluated by MTS colorimetry and AM (a nonfluorescent cell permeability compound) fluorescence method (Fig. 9d). The MTS detection results showed that MC3T3-E1 metabolizes MTS into brown methylamine products in PHC-K9 and that the metabolic value changes with time. The proliferation ability of osteoblasts cultured with PHC-K9 was greater than that of the osteoblasts cultured with PVA after 4 and 7 d, with the greatest increase of 282.19 ± 10.63 % at 10 days. The proliferation ability of the osteoblasts cultured with PHC-P9 exhibited the same trend, with the greatest increase of 229.15 ± 15.14 % at 10 days while that of the osteoblasts cultured with PVA reached the greatest increase of 163.62 ± 10.86 % at 10 days. The proliferation ability of the bone tissue engineering scaffolds prepared with modified nano dispersants was greater than that of the bone tissue engineering scaffolds with unmodified dispersants.

This experiment was through the hydrolysis of calcein AM by an intracellular esterase, to generate strongly green, fluorescent calcein. During the 10-day culture process, MC3T3-E1 osteoblasts grown on PHC-K9 and PHC-P9 had a high survival rate and active cell growth (Fig. 9e). With the increase of culture time, the cells exhibited colony growth morphology and were distributed evenly. In contrast, the cells on the surface of PVA exhibited obvious phenotypes. The cytoplasm of the cells was green spots, round, and less elongated. In terms of cell structure, MC3T3-E1 cells spread on the PHC-K9 scaffold on the 7th and 10th days, and the cells fully grew and proliferated. The cells are long and extend to adjacent areas. The proliferation morphology of MC3T3- E1 cells grown on PHC-K9 and PHC-P9 scaffolds for 4, 7, and 10 d showed that the cells grew in good condition. The fluorescence pattern of MC3T3-E1 cells was consistent with that of proliferating cells, indicating that the PHC-K9 scaffold promoted the growth of osteoblasts during the extended incubation period. In the study of cell viability, compared with the PVA scaffold, HA in the form of modified biological dispersant/HA in the bone tissue engineering scaffold significantly improved the growth, proliferation, and differentiation of osteoblasts, which was consistent with the previously reported scaffold effect of HA on the proliferation of scaffold cells [72,73].

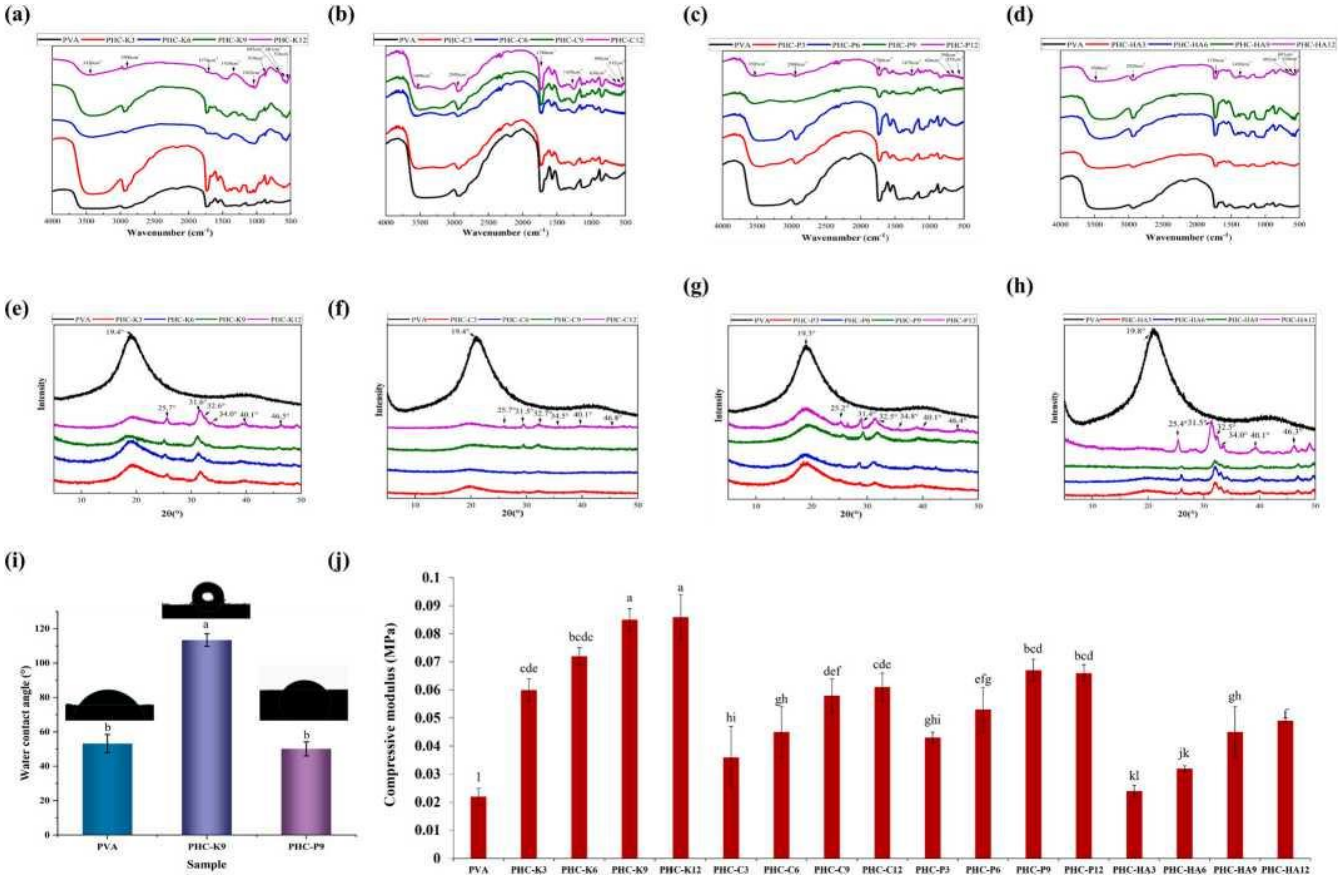

Fig. 8. Structural properties and mechanical characterization of the scaffolds. FTIR analysis of the scaffolds, (a) PHC-K, (b) PHC-C, (c) PHC-P, (d) PHC-HA, XRD analysis of the scaffolds, (e) PHC-K, (f) PHC-C, (g) PHC-P, (h) PHC-HA, water contact angle analysis of PVA, PHC-K9, and PHC-P9 (i), and the compressive modulus of the scaffolds (j). Abbreviations in the figure are as follows: PHC-K (hydroxyapatite synthesized with K-PCNCs as a dispersant/polyvinyl alcohol composite scaffolds), PHC-C (hydroxyapatite synthesized with CCNCs as a dispersant/polyvinyl alcohol composite scaffolds), PHC-P (hydroxyapatite synthesized with PCNCs as a dispersant/polyvinyl alcohol composite scaffolds), PHC-HA (commercial hydroxyapatite/polyvinyl alcohol composite scaffolds). 3, 6, 9, and 12 % were the additional amounts of hydroxyapatite in the composite scaffolds. Different letters (a-l) indicate significant differences between values ($p < 0.05$).

In some studies, HA has been used in polylactic acid [74], CNCs, and PVA. The proportion of cells surviving on PHC-K9 and PHC-P9 was 2 times higher than that on PVA. Bio dispersants can change the complex porous structure of a scaffold and increase osteoblast attachment and proliferation. The membrane permeability and nanostructure also affected osteoblast survival on the scaffold.

The nanoscale HA has the nanostructure composition of the CNCs, and the combination of these water-dispersible material scaffolds, which was helpful for the growth of bone tissue matrix through ionic forces and hydrogen bonds. Molecules containing calcium and phosphorus promoted the adsorption of various proteins [75]. PVA has strong hydrophilicity. Hydrophilicity is an important impact indicator of the ability of nutrients to adhere to cells, and PVA is localized in protein absorption, which promotes the formation of bone tissue matrix [74]. The results for osteoblasts cultured on PHC-K9 and PVA scaffolds showed that the biocompatibility of CNCs and nano HA synthetic scaffolds was improved compared with the PVA scaffold. The scaffold has a complex porous structure, which was conducive to the deep growth of osteoblasts in the porous and has the potential for biological application as a bone tissue engineering material.

ALP ANALYSIS OF BONE TISSUE ENGINEERING SCAFFOLDS

Mineralization of the cells on the three scaffolds was detected on the 4 to 14 d of culture in differentiation medium (Fig. 9f). The activity of ALP released by osteoblasts grown on each scaffold material is different, and the proliferation and differentiation ability of osteoblasts in the PHC-K9 scaffold was stronger. Compared with PHC-K9, the mineralization degree of PVA scaffold material was lower within 14 d of culture, while the ALP activity of PHC-K9 was 0.59 ± 0.09 (ALP activity/mg protein) at the 4th day, reached a peak of 1.71 ± 0.25 (ALP activity/mg protein) at the 14th day; the ALP activity of PHC-P9 was 0.44 ± 0.18 (ALP activity/mg protein) at the 4th day, reached a peak of 1.36 ± 0.17 (ALP activity/mg protein) at the 14th day, while the ALP activity of PVA was 0.22 ± 0.08 (ALP activity/mg protein) at the 4th day, reached a small peak of 0.33 ± 0.07 (ALP activity/mg protein). ALP activity in PHC-K9 gradually increased at the initial stage of culture and increased after 4 days of culture. The existence of ALP activity in osteoblasts enhanced the osteogenic potential of these scaffolds. ALP was very important for the formation of bone tissue matrix in the process of bone repair. It can hydrolyze coll phosphate and provide inorganic phosphorus [76]. It was necessary to synthesize HA, a bone mineralizing substance and was the main regulator of bone tissue mineralization. A small amount of bone ALP will be released into the blood. Bone ALP has high specificity in reflecting osteoblast activity and bone formation, and its role was better than osteocalcin. Therefore, ALP was a differentiation marker that promotes osteogenic differentiation and mineralization expressed by osteoblasts. The proliferation and flattened differentiation of osteoblasts observed on PHC-K9 were due to the characteristic bone tissue components in the scaffold inducing increased cell activity. Many studies have shown that HA can manufacture bone tissue engineering scaffolds [77,78]. By preparing HA on dispersant to simulate bone mineral matrix, CNCs promoted mineralization and formation of new bone. Compared with PVA, the results of cell mineralization observed on the PHC-K9 scaffold were significantly higher.

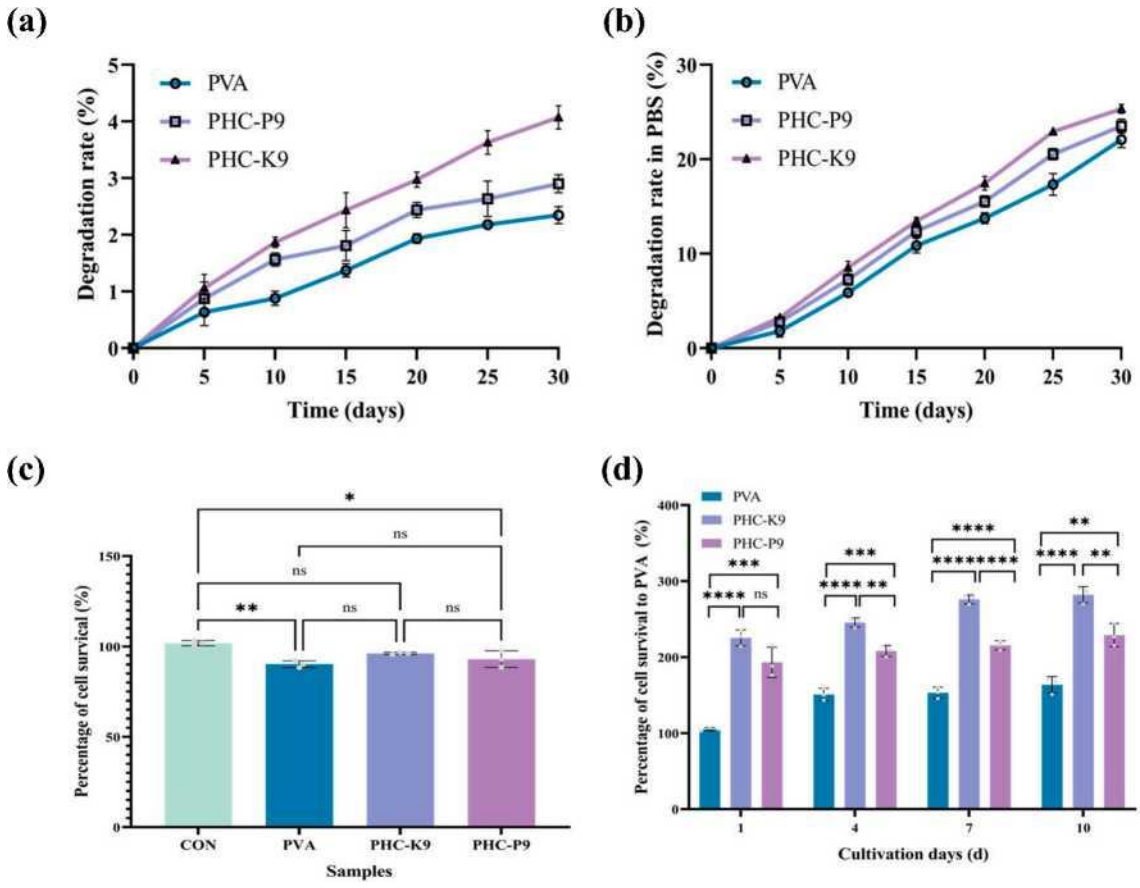

Fig. 9. Characterization of in vitro degradability, biocompatibility, and mineralization properties of screened optimal scaffolds (PVA, PHC-P9, PHC-K9). In vitro degradability of PVA, PHC-P9, PHC-K9 scaffolds in 10 wt% of H_2O_2 (a) and PBS buffer (b), cytotoxicity on the PVA, PHC-P9, PHC-K9 scaffold proliferation of osteoblast MC3T3-E1 (c), cell proliferation of osteoblast MC3T3-E1 on PVA, PHC-P9, PHC-K9 scaffold for 10 days cultivation (d), live/dead cell of osteoblast MC3T3- E1 on PVA, PHC-P9, and PHC-K9 scaffold by fluorescence figure at 4, 7, 10, and 14 days of incubation (e) (scale bar: 50 μm), and ALP activity (nmol/min/mg protein) of osteoblast cells MC3T3-E1 on PVA, PHC-P9, and PHC-K9 scaffold for 14 days cultivation (f). Abbreviations in the figure are as follows: PVA, (polyvinyl alcohol scaffold), PHC-K9 (9% addition amounts of hydroxyapatite The use of 9 % HC-K synthesized with K-PCNCs as a dispersant/polyvinyl alcohol composite scaffolds), PHC-P9 (9% addition amounts of hydroxyapatite synthesized with PCNCs as a dispersant/polyvinyl alcohol composite scaffolds). Results were analyzed between groups (*p <0.05, **p <0.01; ***p <0.001, ****p <0.0001) using one-way ANOVA followed by post-hoc Tukey's test in GraphPad Prism 9.

The use of 9% HC-K increased the biological hardness and provided biomechanical insight into cell attachment because cells prefer to differentiate and proliferate on harder materials.

Conclusions

This study optimized the preparation of alkylation-modified CNCs (K-PCNCs) by analyzing the effect of single factors: ultrasonic treatment time (0-3 h) and ultrasonic treatment power (400-500 W) on the water contact angles (WCA) and the degree of substitution (DS). With ultrasonic treatment of 450 W and 2 h, the WCA and DS of K-PCNCs reached the maximum values (135° and 1.53). In addition, the K-PCNCs had a rod-like structure with a diameter of 28-35 nm and a length of 100-250 nm and had the highest absolute zeta potential (-42.6 ± 0.9 mV), thermal properties (424.57 °C), crystallinity (65.4 ± 4.2°), and dispersing properties, could be used as a dispersant for nanohydroxyapatite (HC-K). Meanwhile, the maximum values of porosity, equilibrium swelling, and mechanical strength (56.1 %, 807.7 %, and 0.085 ± 0.004 MPa, respectively) of the PVA/HA scaffold were obtained at 9 % (w/w) of HC-K addition content. The scaffold promoted osteoblast proliferation and adhesion within 10 d and had a high alkaline phosphatase level (1.71 ± 0.25 ALP activity/mg protein) within 14 days that promoted osteoblast mineralization. The alkylation-modified CNCs significantly improved the dispersion and crystallization properties of the HC-K, as well as the mechanical properties and bone-enhancing ability of the scaffold. These results will help to carry out research on the application of CNCs in the field of bone defect repair and promote innovative applications of different bone tissue engineering scaffolds while emphasizing the importance of balancing physical and biological factors for successful bone formation. In this work, we concluded that the prepared scaffold can be used as a high-potential biomedical scaffold for hard tissue regeneration. However, the mechanical strength and infection resistance of the composite scaffolds as well as the achievement of large-scale commercial applications remain a challenge, and the personalization of large-segment bone defect repairs using bio scaffolds remains a focus of future research.

CRediT authorship contribution statement

Shunshun Zhu: Writing - original draft, Investigation, Formal analysis, Data curation. **Hongnan Sun:** Writing - review & editing, Visualization, Validation, Supervision, Methodology. **Taihua Mu:** Writing - review & editing, Supervision, Conceptualization. **Aurore Richel:** Writing - review & editing, Conceptualization.

Declaration of competing interest

The authors declare that they have no known competing financial interests or personal relationships that could have appeared to influence the work reported in this paper.

DATA AVAILABILITY

Data will be made available on request.

ACKNOWLEDGMENTS

The authors gratefully acknowledge the earmarked fund for CARS (CARS-10), and the Science and Technology Innovation Project of the Chinese Academy of Agricultural Sciences (CAAS-ASTIP-202X-IFST).

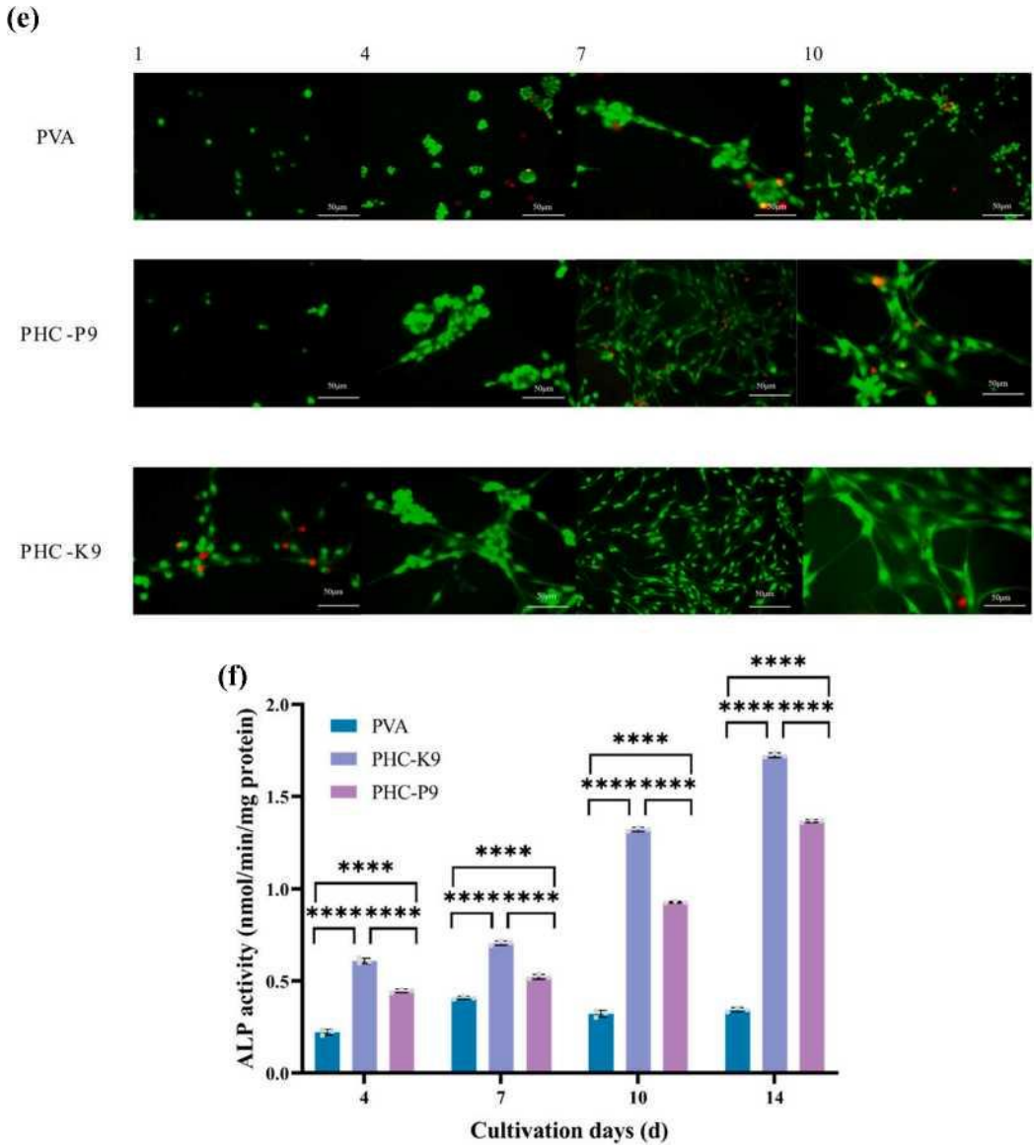

Fig. 9. (*continued*).

APPENDIX A. SUPPLEMENTARY DATA

Supplementary data to this article can be found online at https://doi.org/10.1016/j.ijbiomac.2024.135571.

References

[1] A.R. Amini, C.T. Laurencin, S.P. Nukavarapu, Bone tissue engineering: recent advances and challenges, Crit. Rev. Biomed. Eng. 40 (2012), https://doi.org/ 10.1615/CritRev-BiomedEng.v40.i5.10.

[2] C. Huang, S. Bhagia, N. Hao, X. Meng, L. Liang, Q. Yong, A.J. Ragauskas, Biomimetic composite scaffold from an in situ hydroxyapatite coating on cellulose nanocrystals, RSC Adv. 9 (2019), https://doi.org/10.1039/c8ra09523j.

[3] H. Ullah, F. Wahid, H.A. Santos, T. Khan, Advances in biomedical and pharmaceutical applications of functional bacterial cellulose-based nanocomposites, Carbohydr. Polym. 150 (2016), https://doi.org/10.1016/j.carbpol.2016.05.029.

[4] S. Chahal, F.S.J. Hussain, A. Kumar, M.S.B.A. Rasad, M.M. Yusoff, Fabrication, characterization and in vitro biocompatibility of electrospun hydroxyethyl cellulose/ poly (vinyl) alcohol nanofibrous composite biomaterial for bone tissue engineering, Chem. Eng. Sci. 144 (2016), https://doi.org/10.1016/j. ces.2015.12.030.

[5] L. Cui, J. Zhang, J. Zou, X. Yang, H. Guo, H. Tian, P. Zhang, Y. Wang, N. Zhang, X. Zhuang, Z. Li, J. Ding, X. Chen, Electroactive composite scaffold with locally expressed osteoinductive factor for synergistic bone repair upon electrical stimulation, Biomaterials 230 (2020), https://doi.org/10.1016/j.biomaterials.2019.119617.

[6] M. Roman, A.P. Haring, T.J. Bertucio, The growing merits and dwindling limitations of bacterial cellulose-based tissue engineering scaffolds, Curr. Opin. Chem. Eng. 24 (2019), https://doi.org/10.1016/j.coche.2019.03.006.

[7] P. Feng, R. Zhao, W. Tang, F. Yang, H. Tian, S. Peng, H. Pan, C. Shuai, Structural and functional adaptive artificial bone: materials, fabrications, and properties, Adv. Funct. Mater. 33 (2023), https://doi.org/10.1002/adfm.202214726.

[8] A. Rahmani Del Bakhshayesh, S. Babaie, H. Tayefi Nasrabadi, N. Asadi, A. Akbarzadeh, A. Abedelahi, An overview of various treatment strategies, especially tissue engineering for damaged articular cartilage, Artif. Cells Nanomed. Biotechnol. 48 (2020), https://doi.org/10.1080/21691401.2020.1809439.

[9] A. Kumar, Y.S. Negi, V. Choudhary, N.K. Bhardwaj, Microstructural and mechanical properties of porous biocomposite scaffolds based on polyvinyl alcohol, nanohydroxyapatite and cellulose nanocrystals, Cellulose 21 (2014), https://doi.org/ 10.1007/s10570-014-0339-7.

[10] A.A. Ashraf, S.M. Zebarjad, M.J. Hadianfard, The cross-linked polyvinyl alcohol/ hydroxyapatite nanocomposite foam, J. Mater. Res. Technol. 8 (2019), https://doi. org/10.1016/j.jmrt.2019.02.024.

[11] L. Yu, D.W. Rowe, I.P. Perera, J. Zhang, S.L. Suib, X. Xin, M. Wei, Intrafibrillar mineralized collagen-hydroxyapatite-based scaffolds for bone regeneration, ACS Appl. Mater. Interfaces 12 (2020), https://doi.org/10.1021/acsami.0c00275.

[12] R. de Santis, A. Russo, A. Gloria, U. D'Amora, T. Russo, S. Panseri, M. Sandri, A. Tampieri, M. Marcacci, V.A. Dediu, C.J. Wilde, L. Ambrosio, Towards the design of 3D fiber-deposited poly(e-caprolactone)/iron-doped hydroxyapatite nanocomposite magnetic scaffolds for bone regeneration, J. Biomed. Nanotechnol. 11 (2015), https://doi.org/10.1166/jbn.2015.2065.

[13] M.A. Irfa'i, W.W. Schmahl, Y.M. Pusparizkita, S. Muryanto, A. Prihanto, R. Ismail, J. Jamari, A.P. Bayuseno, Hydrothermally synthesized-nanoscale carbonated hydroxyapatite with calcium carbonates derived from green mussel shell wastes, J. Mol. Struct. 1306 (2024), https://doi.org/10.1016/j.molstruc.2024.137837.

[14] S.Y. Peng, Y.W. Lin, Y.Y. Lin, K.L. Lin, Hydrothermal synthesis of hydroxyapatite nanocrystals from calcium-rich limestone sludge waste: preparation, characterization, and application for Pb^{2+} adsorption in aqueous solution, Inorg. Chem. Commun. 160 (2024), https://doi.org/10.1016/j.inoche.2023.111943.

[15] K. Lee, K.Y. Kwon, Preparation of amine-incorporated hydroxyapatite through a single-step hydrothermal reaction, Mater. Lett. 355 (2024), https://doi.org/ 10.1016/j.matlet.2023.135508.

[16] S. Pang, H. An, X. Zhao, Y. Wang, Ionic liquid-assisted preparation of hydroxyapatite and its catalytic performance for decarboxylation of itaconic acid, Chin. J. Chem. Eng. 67 (2024), https://doi.org/10.1016/j.cjche.2023.11.018.

[17] N. Abdian, M. Etminanfar, S.O.R. Sheykholeslami, H. Hamishehkar, J. Khalil-Allafi, Preparation and characterization of chitosan/hydroxyapatite scaffolds containing mesoporous SiO_2-HA for drug delivery applications, Mater. Chem. Phys. 301 (2023), https://doi.org/10.1016/j.matchemphys.2023.127672.

[18] L. Wan, B. Cui, L. Wang, A review on preparation raw materials, synthesis methods, and modifications of hydroxyapatite as well as their environmental applications, Sustain. Chem. Pharm. 38 (2024), https://doi.org/10.1016/j.scp.2024.101447.

[19] S. Sebastiammal, A.S.L. Fathima, K.A. Al-Ghanim, M. Nicoletti, G. Baskar, J. Iyyappan, M. Govindarajan, Synthesis and characterization of magnesium- wrapped hydroxyapatite nanomaterials for biomedical applications, Surf. Interfaces 44 (2024), https://doi.org/10.1016/j.surfin.2023.103779.

[20] S.H. Zainal, N.H. Mohd, N. Suhaili, F.H. Anuar, A.M. Lazim, R. Othaman, Preparation of cellulose-based hydrogel: a review, J. Mater. Res. Technol. 10 (2021), https://doi.org/10.1016/j.jmrt.2020.12.012.

[21] H. Seddiqi, E. Oliaei, H. Honarkar, J. Jin, L.C. Geonzon, R.G. Bacabac, J. Klein- Nulend, Cellulose and its derivatives: towards biomedical applications, Cellulose 28 (2021) 1893-1931, https://doi.org/10.1007/s10570-020-03674-w.

[22] P. Panyasiri, N.T. Lam, P. Sukyai, The effect of hydroxyapatite prepared by in situ synthesis on the properties of poly(vinyl alcohol)/cellulose nanocrystals biomaterial, J. Polym. Environ. 28 (2020), https://doi.org/10.1007/s10924-019-01599-5.

[23] N. Grishkewich, N. Mohammed, J. Tang, K.C. Tam, Recent advances in the application of cellulose nanocrystals, Curr. Opin. Colloid Interface Sci. 29 (2017), https://doi.org/10.1016/j.cocis.2017.01.005.

[24] N.T. Lam, R. Chollakup, W. Smitthipong, T. Nimchua, P. Sukyai, Characterization of cellulose nanocrystals extracted from sugarcane bagasse for potential biomedical materials, Sugar Tech 19 (2017), https://doi.org/10.1007/s12355-016-0507-1.

[25] T. Niamsap, N.T. Lam, P. Sukyai, Production of hydroxyapatite-bacterial nanocellulose scaffold with assist of cellulose nanocrystals, Carbohydr. Polym. 205 (2019), https://doi.org/10.1016/j.carbpol.2018.10.034.

[26] M. Ly, T.H. Mekonnen, Cationic surfactant modified cellulose nanocrystals for corrosion protective nanocomposite surface coatings, J. Ind. Eng. Chem. 83 (2020), https://doi.org/10.1016/j.jiec.2019.12.014.

[27] M. Manimaran, M.N. Norizan, M.H. Mohamad Kassim, M.R. Adam, M.N. F. Norrrahim, V.F. Knight, Critical assessment of the thermal stability and degradation of chemically functionalized nanocellulose-based polymer nanocomposites, Nanotechnol. Rev. 13 (2024), https://doi.org/10.1515/ntrev- 2024-0005.

[28] F. D'Acierno, I. Capron, Modulation of surface properties of cellulose nanocrystals through adsorption of tannic acid and alkyl cellulose derivatives, Carbohydr. Polym. 319 (2023), https://doi.org/10.1016/j.carbpol.2023.121159.

[29] X. Shi, X. Qin, Y. Dai, X. Liu, W. Wang, J. Zhong, Improved catalytic properties of Candida antarctica lipase B immobilized on cetyl chloroformate-modified cellulose nanocrystals, Int. J. Biol. Macromol. 220 (2022), https://doi.org/10.1016/j. ijbiomac.2022.08.170.

[30] E. Esmizadeh, A. Gupta, S. Asrat, T.H. Mekonnen, Crystallization and performance evolution of PHBV nanocomposites through annealing: the role of surface modification of CNCs, Polymer 308 (2024), https://doi.org/10.1016/j. polymer.2024.127352.

[31] Q. Wu, J. Xu, Z. Wu, S. Zhu, Y. Gao, C. Shi, The effect of surface modification on chemical and crystalline structure of the cellulose III nanocrystals, Carbohydr. Polym. 235 (2020),

https://doi.org/10.1016/j.carbpol.2020.115962.

[32] E. Abraham, D.E. Weber, S. Sharon, S. Lapidot, O. Shoseyov, Multifunctional cellulosic scaffolds from modified cellulose nanocrystals, ACS Appl. Mater. Interfaces 9 (2017), https://doi.org/10.1021/acsami.6b13528.

[33] J.A. Ávila Ramírez, C. G**o**mez Hoyos, S. Arroyo, P. Cerrutti, M.L. Foresti, Naturally occurring?-hydroxy acids: useful organocatalysts for the acetylation of cellulose nanofibres, Curr. Organocatal. 3 (2015) 28232503, https://doi.org/10.2174/ 22133372026661504.

[34] H. Kang, R. Liu, Y. Huang, Graft modification of cellulose: methods, properties and applications, Polymer 70 (2015), https://doi.org/10.1016/j.polymer.2015.05.041.

[35] Z. Liu, K. Khurshid, M.D.A. Saldaña, Hydrogels and aerogels of cellulose nanofiber derived from barley straw with addition of chitosan using high-intensity ultrasound and supercritical CO2 drying, Ind. Crop. Prod. 216 (2024), https://doi.org/10.1016/j.indcrop.2024.118755.

[36] N. Thirunavookarasu, S. Kumar, P. Shetty, A. Shanmugam, A. Rawson, Impact of ultrasound treatment on the structural modifications and functionality of carbohydrates - a review, Carbohydr. Res. 535 (2024), https://doi.org/10.1016/j. carres.2023.109017.

[37] A.L.R. Costa, A. Gomes, H. Tibolla, F.C. Menegalli, R.L. Cunha, Cellulose nanofibers from banana peels as a Pickering emulsifier: high-energy emulsification processes, Carbohydr. Polym. 194 (2018), https://doi.org/10.1016/j.carbpol.2018.04.001.

[38] S. Zhu, H. Sun, T. Mu, Q. Li, A. Richel, Preparation of cellulose nanocrystals from purple sweet potato peels by ultrasound-assisted maleic acid hydrolysis, Food Chem. 403 (2023), https://doi.org/10.1016/j.foodchem.2022.134496.

[39] N. Tien Lam, V. Minh Quan, S. Boonrungsiman, P. Sukyai, Effectiveness of biodispersant in homogenizing hydroxyapatite for proliferation and differentiation of osteoblast, J. Colloid Interface Sci. 611 (2022), https://doi.org/10.1016/j. jcis.2021.12.088.

[40] W. Lan, X. Zhang, M. Xu, L. Zhao, D. Huang, X. Wei, W. Chen, Carbon nanotube reinforced polyvinyl alcohol/biphasic calcium phosphate scaffold for bone tissue engineering, RSC Adv. 9 (2019), https://doi.org/10.1039/c9ra08569f.

[41] M. Sukul, P. Sahariah, H.L. Lauzon, J. Borges, M. M**o**asson, J.F. Mano, H.J. Haugen, J.E. Reseland, In vitro biological response of human osteoblasts in 3D chitosan sponges with controlled degree of deacetylation and molecular weight, Carbohydr. Polym. 254 (2021) 117434, https://doi.org/10.1016/j.carbpol.2020.117434.

[42] A. Giubilini, M. Messori, F. Bondioli, P. Minetola, L. luliano, G. Nystr**o**m, K. Maniura-Weber, M. Rottmar, G. Siqueira, 3D-printed poly(3-hydroxybutyrate- co-3-hydroxyhexanoate)-cellulose-based scaffolds for biomedical applications, Biomacromolecules 24 (2023) 3961-3971, https://doi.org/10.1021/acs. biomac.3c00263.

[43] R. Morsy, Development and characterization of antibacterial 3D porous hydroxyapatite-gelatin-PVA scaffolds containing zinc oxide nanoparticles, Mater. Chem. Phys. 314 (2024), https://doi.org/10.1016/j.matchemphys.2023.128831.

[44] T. Ma, X. Hu, S. Lu, R. Cui, J. Zhao, X. Hu, Y. Song, Cellulose nanocrystals produced using recyclable sulfuric acid as hydrolysis media and their wetting molecular dynamics simulation, Int. J. Biol. Macromol. 184 (2021) 405-414, https://doi.org/ 10.1016/j.ijbiomac.2021.06.094.

[45] A.A.D. Meirelles, A.L.R. Costa, R.L. Cunha, Cellulose nanocrystals from ultrasound process stabilizing O/W Pickering emulsion, Int. J. Biol. Macromol. 158 (2020), https://doi.org/10.1016/j.ijbiomac.2020.04.185.

[46] A.L.R. Costa, A. Gomes, G. de F. Furtado, H. Tibolla, F.C. Menegalli, R.L. Cunha, Modulating in vitro digestibility of Pickering emulsions stabilized by food-grade polysaccharides particles, Carbohydr. Polym. 227 (2020), https://doi.org/ 10.1016/j.carbpol.2019.115344.

[47] Z. Wu, J. Xu, J. Gong, J. Li, L. Mo, Preparation, characterization and acetylation of cellulose

nanocrystal allomorphs, Cellulose 25 (2018) 4905-4918, https://doi.org/ 10.1007/s10570-018-1937-6.

[48] A. Lepetit, R. Drolet, B. Tolnai, D. Montplaisir, R. Zerrouki, Alkylation of microfibrillated cellulose - a green and efficient method for use in fiber-reinforced composites, Polymer (2017), https://doi.org/10.1016/j.polymer.2017.08.024.

[49] K.J. Nagarajan, A.N. Balaji, S. Thanga Kasi Rajan, K. Sathick Basha, Effect of sulfuric acid reaction time on the properties and behavior of cellulose nanocrystals from Cocos nucifera var-Aurantiaca peduncle's cellulose microfibers, Mater. Res. Express 6 (2019), https://doi.org/10.1088/2053-1591/ab5a9d.

[50] H. Jiang, S. Wu, J. Zhou, Preparation and modification of nanocellulose and its application to heavy metal adsorption: a review, Int. J. Biol. Macromol. 236 (2023), https://doi.org/10.1016/j.ijbiomac.2023.123916.

[51] J. Guo, X. Guo, S. Wang, Y. Yin, Effects of ultrasonic treatment during acid hydrolysis on the yield, particle size and structure of cellulose nanocrystals, Carbohydr. Polym. 135 (2016) 248-255, https://doi.org/10.1016/j. carbpol.2015.08.068.

[52] J. Lu, P. Askeland, L.T. Drzal, Surface modification of microfibrillated cellulose for epoxy composite applications, Polymer 49 (2008), https://doi.org/10.1016/j. polymer.2008.01.028.

[53] Y. Shih, C. Huang, P. Chen, Biodegradable green composites reinforced by the fiber recycling from disposable chopsticks, Mater. Sci. Eng., A 527 (2010) 1516-1521, https://doi.org/10.1016/j.msea.2009.10.024.

[54] M.L. Chinta, A. Velidandi, N.P.P. Pabbathi, S. Dahariya, S.R. Parcha, Assessment of properties, applications and limitations of scaffolds based on cellulose and its derivatives for cartilage tissue engineering: a review, Int. J. Biol. Macromol. 175 (2021), https://doi.org/10.1016/j.ijbiomac.2021.01.196.

[55] K. Li, S. Jin, F. Zhang, Y. Zhou, G. Zeng, J. Li, S.Q. Shi, J. Li, Bioinspired phenolamine chemistry for developing bioadhesives based on biomineralized cellulose nanocrystals, Carbohydr. Polym. 296 (2022), https://doi.org/10.1016/j.carbpol.2022.119892.

[56] A.Y. Melikoğlu, S.E. Bilek, S. Cesur, Optimum alkaline treatment parameters for the extraction of cellulose and production of cellulose nanocrystals from apple

pomace, Carbohydr. Polym. 215 (2019) 330-337, https://doi.org/10.1016/j. carbpol.2019.03.103.

[57] L. Wang, Y. Li, L. Ye, C. Zhi, T. Zhang, M. Miao, Unveiling structure and performance of tea-derived cellulose nanocrystals, Int. J. Biol. Macromol. 270 (2024), https://doi.org/10.1016/j.ijbiomac.2024.132117.

[58] M. Roman, W.T. Winter, Effect of sulfate groups from sulfuric acid hydrolysis on the thermal degradation behavior of bacterial cellulose, Biomacromolecules 5 (2004), https://doi.org/10.1021/bm034519+.

[59] M.A. Torlopov, I.S. Martakov, V.I. Mikhaylov, K.A. Cherednichenko, P. Sitnikov, Synthesis and properties of thiol-modified CNC via surface tosylation, Carbohydr. Polym. 319 (2023), https://doi.org/10.1016/j.carbpol.2023.121169.

[60] C. Shuai, W. Yang, P. Feng, S. Peng, H. Pan, Accelerated degradation of HAP/PLLA bone scaffold by PGA blending facilitates bioactivity and osteoconductivity, Bioact. Mater. 6 (2021), https://doi.org/10.1016/j.bioactmat.2020.09.001.

[61] M. Bakkari, V. Bindiganavile, Y. Boluk, Facile synthesis of calcium hydroxide nanoparticles onto tempo-oxidized cellulose nanofibers for heritage conservation, ACS Omega 4 (2019), https://doi.org/10.1021/acsomega.9b02643.

[62] P. Deb, S. Das Lala, E. Barua, A.B. Deoghare, Physico-mechanical and biological analysis of composite bone scaffold developed from catla catla fish scale derived hydroxyapatite for bone tissue engineering, Arab. J. Sci. Eng. 49 (2024), https:// doi.org/10.1007/s13369-023-07872-z.

[63] L. Zhang, T. Lu, F. He, W. Zhang, X. Yuan, X. Wang, J. Ye, Physicochemical and cytological

properties of poorly crystalline calcium-deficient hydroxyapatite with different ca/P ratios, Ceram. Int. 48 (2022), https://doi.org/10.1016/j.ceramint.2022.05.126.

[64] R. Li, J. Fei, Y. Cai, Y. Li, J. Feng, J. Yao, Cellulose whiskers extracted from mulberry: a novel biomass production, Carbohydr. Polym. 76 (1) (2009) 94-99, https://doi.org/10.1016/j.carbpol.2008.09.034.

[65] E. Daldiken, F.Z. Koçak, N. Küçükdeveci, Synthesis and characterizations of clinoptilolite enriched hydroxyapatite nanoceramics by sol-gel route for bone regeneration, Ceram. Int. 50 (2024), https://doi.org/10.1016/j.ceramint.2024.03.084.

[66] M.J. Abden, J.D. Afroze, M.S. Alam, N.M. Bahadur, Pressure less sintering and mechanical properties of hydroxyapatite/functionalized multi-walled carbon nanotube composite, Mater. Sci. Eng. C 67 (2016), https://doi.org/10.1016/j. msec.2016.05.018.

[67] C. Shuai, B. Peng, P. Feng, L. Yu, R. Lai, A. Min, In situ synthesis of hydroxy- apatite nanorods on graphene oxide nanosheets and their reinforcement in biopolymer scaffold, J. Adv. Res. 35 (2022), https://doi.org/10.1016/j.jare.2021.03.009.

[68]C. Shuai, X. Shi, K. Wang, Y. Gu, F. Yang, P. Feng, Ag-doped CNT/HAP nanohybrids in a PLLA bone scaffold show significant antibacterial activity, Biodes. Manuf. 7 (2024), https://doi.org/10.1007/s42242-023-00264-0.

[69]M. Avella, M. Cocca, M.E. Errico, G. Gentile, Polyvinyl alcohol biodegradable foams containing cellulose fibers, J. Cell. Plast. (2012), https://doi.org/10.1177/ 0021955X1244 9639.

[70]P. Ma, W. Wu, Y. Wei, L. Ren, S. Lin, J. Wu, Biomimetic gelatin/chitosan/polyvinyl alcohol/nano-hydroxyapatite scaffolds for bone tissue engineering, Mater. Des. 207 (2021), https://doi.org/10.1016/j.matdes.2021.109865.

[71]S. Dong, A.A. Hirani, K.R. Colacino, Y.W. Lee, M. Roman, Cytotoxicity and cellular uptake of cellulose nanocrystals, Nano Life 02 (2012), https://doi.org/10.1142/ s1793 984412410061.

[72]X.Y. Zhang, Y.P. Chen, J. Han, J. Mo, P.F. Dong, Y.H. Zhuo, Y. Feng, Biocompatible silk fibroin/carboxymethyl chitosan/strontium substituted hydroxyapatite/ cellulose nanocrystal composite scaffolds for bone tissue engineering, Int. J. Biol. Macromol. 136 (2019), https://doi.org/10.1016/j.ijbiomac.2019.06.172.

[73] T. Osathanon, C.M. Giachelli, M.J. Somerman, Immobilization of alkaline phosphatase on microporous nanofibrous fibrin scaffolds for bone tissue engineering, Biomaterials 30 (2009), https://doi.org/10.1016/j.biomaterials.2009.05.022.

[74]A. Abdal-Hay, F.A. Sheikh, J.K. Lim, Air jet spinning of hydroxyapatite/poly(lactic acid) hybrid nanocomposite membrane mats for bone tissue engineering, Colloids Surf. B Biointerfaces 102 (2013), https://doi.org/10.1016/j.colsurfb.2012.09.017.

[75]X. Sun, X. Yang, Y. Su, M. Teng, J. Liao, A. Niu, X. Liang, Morphology improvement of sandblasted and acid-etched titanium surface and osteoblast attachment promotion by hydroxyapatite coating, Rare Metal Mater. Eng. 44 (2015), https:// doi.org/10.1016/s1875-5372(15)30014-x.

[76]D.K. Patel, S.D. Dutta, J. Hexiu, K. Ganguly, K.T. Lim, 3D-printable chitosan/silk fibroin/cellulose nanoparticle scaffolds for bone regeneration via M2 macrophage polarization, Carbohydr. Polym. 281 (2022), https://doi.org/10.1016/j.carbpol.2021.119077.

[77]J. Prakash, D. Prema, K.S. Venkataprasanna, K. Balagangadharan,

N. Selvamurugan, G.D. Venkatasubbu, Nanocomposite chitosan film containing graphene oxide/hydroxyapatite/gold for bone tissue engineering, Int. J. Biol. Macromol. 154 (2020), https://doi.org/10.1016/j.ijbiomac.2020.03.095.

[78]R. Budiraharjo, K.G. Neoh, E.T. Kang, Hydroxyapatite-coated carboxymethyl chitosan scaffolds for promoting osteoblast and stem cell differentiation, J. Colloid Interface Sci. 366 (2012), https://doi.org/10.1016/j.jcis.2011.09.072.